1-1-2007

On the duration of magnetochrons C24r and C25n and the timing of early Eocene global warming events: Implications from the Ocean Drilling Program Leg 208 Walvis Ridge depth transect

Thomas Westerhold
Bremen University

Ursula Röhl
Bremen University

Jacques Laskar
IMCCE-CNRS UMR

Isabella Raffi
Università degli Studi "G. d'Annunzio" Chieti-Pescara

Julie A. Bowles
University of Wisconsin-Milwaukee, bowlesj@uwm.edu

See next page for additional authors

Authors
Thomas Westerhold, Ursula Röhl, Jacques Laskar, Isabella Raffi, Julie A. Bowles, Lucas J. Lourens, and James C. Zachos

PALEOCEANOGRAPHY, VOL. 22, PA2201, doi:10.1029/2006PA001322, 2007

On the duration of magnetochrons C24r and C25n and the timing of early Eocene global warming events: Implications from the Ocean Drilling Program Leg 208 Walvis Ridge depth transect

Thomas Westerhold,[1] Ursula Röhl,[1] Jacques Laskar,[2] Isabella Raffi,[3] Julie Bowles,[4] Lucas J. Lourens,[5] and James C. Zachos[6]

Received 18 May 2006; revised 10 October 2006; accepted 6 November 2006; published 6 April 2007.

[1] Five sections drilled in multiple holes over a depth transect of more than 2200 m at the Walvis Ridge (SE Atlantic) during Ocean Drilling Program (ODP) Leg 208 resulted in the first complete early Paleogene deep-sea record. Here we present high-resolution stratigraphic records spanning a ~4.3 million yearlong interval of the late Paleocene to early Eocene. This interval includes the Paleocene-Eocene thermal maximum (PETM) as well as the Eocene thermal maximum (ETM) 2 event. A detailed chronology was developed with nondestructive X-ray fluorescence (XRF) core scanning records and shipboard color data. These records were used to refine the shipboard-derived spliced composite depth for each site and with a record from ODP Site 1051 were then used to establish a continuous time series over this interval. Extensive spectral analysis reveals that the early Paleogene sedimentary cyclicity is dominated by precession modulated by the short (100 kyr) and long (405 kyr) eccentricity cycles. Counting of precession-related cycles at multiple sites results in revised estimates for the duration of magnetochrons C24r and C25n. Direct comparison between the amplitude modulation of the precession component derived from XRF data and recent models of Earth's orbital eccentricity suggests that the onset of the PETM and ETM2 are related to a 100-kyr eccentricity maximum. Both events are approximately a quarter of a period offset from a maximum in the 405-kyr eccentricity cycle, with the major difference that the PETM is lagging and ETM2 is leading a 405-kyr eccentricity maximum. Absolute age estimates for the PETM, ETM2, and the magnetochron boundaries that are consistent with recalibrated radiometric ages and recent models of Earth's orbital eccentricity cannot be precisely determined at present because of too large uncertainties in these methods. Nevertheless, we provide two possible tuning options, which demonstrate the potential for the development of a cyclostratigraphic framework based on the stable 405-kyr eccentricity cycle for the entire Paleogene.

Citation: Westerhold, T., U. Röhl, J. Laskar, I. Raffi, J. Bowles, L. J. Lourens, and J. C. Zachos (2007), On the duration of magnetochrons C24r and C25n and the timing of early Eocene global warming events: Implications from the Ocean Drilling Program Leg 208 Walvis Ridge depth transect, *Paleoceanography*, *22*, PA2201, doi:10.1029/2006PA001322.

1. Introduction

[2] Over the last decade significant progress has been made in the construction of astronomically calibrated geological timescales for the Neogene and late Paleogene [e.g., *Hilgen et al.*, 1999; *Shackleton et al.*, 1999] and the development of high-resolution paleoceanographic records. These successes have encouraged efforts to extend the astronomical calibration to older successions including the warm greenhouse periods of the Eocene. However, extending astronomically calibrated timescales into the early Paleogene faces fundamental problems that are related to uncertainties of astronomical calculations [*Laskar*, 1999] and to the sensitivity of a climate system under very different boundary conditions (i.e., more pCO_2, less ice), as well as the unavailability of stratigraphically complete and undisturbed sedimentary successions of this age [*Cramer et al.*, 2003; *Tripati et al.*, 2003]. Nonetheless, some progress has been made in both minimizing the uncertainties, and obtaining sequences suitable for astronomical calibration.

[3] Extending the astronomical calibration into the early Paleogene will provide new insight for resolving rates of paleoceanographic change associated with the abrupt, short-lived events like the PETM [*Kennett and Stott*, 1991; *Koch et al.*, 1992; *Zachos et al.*, 2005] and the ETM2 [*Lourens et al.*, 2005]. Although it seems to be clear that these Events are astronomically paced [*Lourens et al.*, 2005], controversy

[1]Centre for Marine Environmental Sciences, Bremen University, Bremen, Germany.
[2]Astronomie et Systèmes Dynamiques, IMCCE-CNRS UMR 8028, Paris, France.
[3]Facoltà di Scienze, Dipartimento di Geotecnologie per l'Ambiente e il Territorio, Università "G. d'Annunzio" di Chieti-Pescara, Chieti Scalo, Italy.
[4]Scripps Institution of Oceanography, University of California, San Diego, La Jolla, California, USA.
[5]Faculty of Geosciences, Department of Earth Sciences, Utrecht University, Utrecht, Netherlands.
[6]Earth and Planetary Sciences Department, University of California, Santa Cruz, California, USA.

0883-8305/07/2006PA001322$12.00

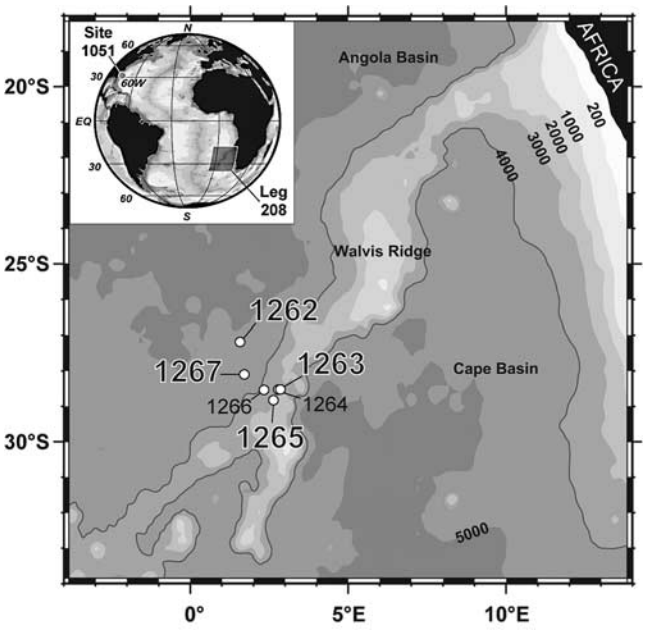

Figure 1. Contour map showing the position of Walvis Ridge ODP Leg 208 sites. The small global map indicates the area represented by the contour map as well as the location of ODP Site 1051 (Blake Nose).

exists whether they are bound to long-term eccentricity maxima [*Lourens et al.*, 2005] or minima [*Cramer et al.*, 2003]. At present it has still been difficult to determine the exact position of the PETM within chron C24r as well as the total duration of this chron itself. So far different approaches have been used to estimate the duration of magnetochron C24r [*Aubry et al.*, 1996; *Berggren and Aubry*, 1996; *Berggren et al.*, 1995; *Cramer*, 2001; *Cramer et al.*, 2003; *Dinarès-Turell et al.*, 2002; *Norris and Röhl*, 1999; *Röhl et al.*, 2000, 2003], including cycle counting at Ocean Drilling Program (ODP) Site 1051 [*Röhl et al.*, 2003] and carbon isotope stacking of multiple DSDP and ODP sites [*Cramer et al.*, 2003], the exact duration is still unknown [*Aubry et al.*, 1996; *Cramer et al.*, 2003; *Raffi et al.*, 2005].

[4] Significant improvements in the chronology of C24r were provided by the successful efforts of ODP Leg 208 (Walvis Ridge [*Zachos et al.*, 2004]), which produced the first complete spliced records or 'composite sections' for the early Paleogene as a result of coring multiple holes at five different sites over a depth transect of more than 2200 m. Because of the exceptional good core recovery, it was possible to resolve the complete spectrum of lithologic variability down to the centimeter scale, including orbital-paced oscillations. As a consequence, Leg 208 documented the occurrence of a number of "critical" events of the early Paleogene, several either previously undocumented or poorly constrained [e.g., *Lourens et al.*, 2005; *Röhl et al.*, 2004, 2005; *Zachos et al.*, 2005]. The primary objective of this study is to establish a precise and continuous cyclostratigraphy for magnetochrons C24r and C25n and the relative timing of the hyperthermals therein. The multiple composite sections and high-resolution records of Leg 208 allow the development of a timescale down to the precession scale. We will make use of long and high-resolution time series of continuous physical and chemical sediment parameters and apply detailed spectral analysis in the depth domain as the first step in timescale construction.

2. Material and Methods

[5] Five Paleocene-Eocene (P-E) boundary sections were recovered in multiple holes over a depth transect of more than 2200 m at the Walvis Ridge (SE Atlantic, Figure 1) during ODP Leg 208, which provide the first complete early Paleogene deep-sea record with moderate to relatively high sedimentation rates (1 to 3 cm/kyr) [*Shipboard Scientific Party*, 2004b]. These records provide a detailed history of paleoceanographic variations associated with several prominent episodes of early Cenozoic climate change, including the Paleocene-Eocene thermal maximum (PETM) [*Zachos et al.*, 2005]), and recently identified transient warming events such as the ETM2. Both events are marked by carbonate dissolution horizons in the Walvis Ridge sediments of which the latter was termed Elmo [*Lourens et al.*, 2005]. For this study we analyzed cores from ODP Sites 1262 (27°11.15′S, 01°34.62′E, 4755 mbsl), 1263 (28°31.98′S, 02°46.77′E, 2717 mbsl), 1265 (28°50.10s, 02°38.35′E, 3060 mbsl), and 1267 (28°05.88′S, 01°42.66′E, 4355 mbsl). In addition, we use data collected from ODP Site 1051 (Leg 171B, Blake Nose, Figure 1) [*Bains et al.*, 2003; *Cramer*, 2001; *Cramer et al.*, 2003; *Norris and Röhl*, 1999; *Röhl et al.*, 2000, 2003].

Figure 2. Composite records of ODP Leg 208 Sites (bottom to top) 1262, 1267, 1265, and 1263 (according to the water depth) versus meters composite depth (mcd) or revised meters composite depth (rmcd). For all four sites, a* (redness over greenness) color values are plotted in black. We plotted in red the magnetic susceptibility (Site 1267) or the Fe intensity from high-resolution XRF logging on a logarithmic scale (Sites 1262, 1265, and 1263). For Sites 1262 and 1267 the position of magnetochron boundaries with error ranges in gray are plotted. The pin with error bars indicate the position of calcareous nannofossils datums (Sites 1267, 1263, and 1265 are revised shipboard data; Site 1262 is new data, this study): Numbers stand for the following: 1, highest occurrence (HO) *D. multiradiatus*; 1a, *D. multiradiatus* decrease; 2, HO *T. contortus*; 3, lowest occurrence (LO) *T. orthostylus*; 4, LO *T. contortus*; 5, LO *D. diastypus*; 6, HO *Fasciculithus* spp.; 7, abundance crossover *Fasculithus*/*Z. bijugatus*; 8, range of *R. calcitrapa* gr.; and 9, LO *D. multiradiatus*. The two blue lines across the four plots mark the position of the Elmo horizon (ETM 2) [*Lourens et al.*, 2005] and the Paleocene-Eocene thermal maximum (PETM, ETM 1) [*Zachos et al.*, 2005].

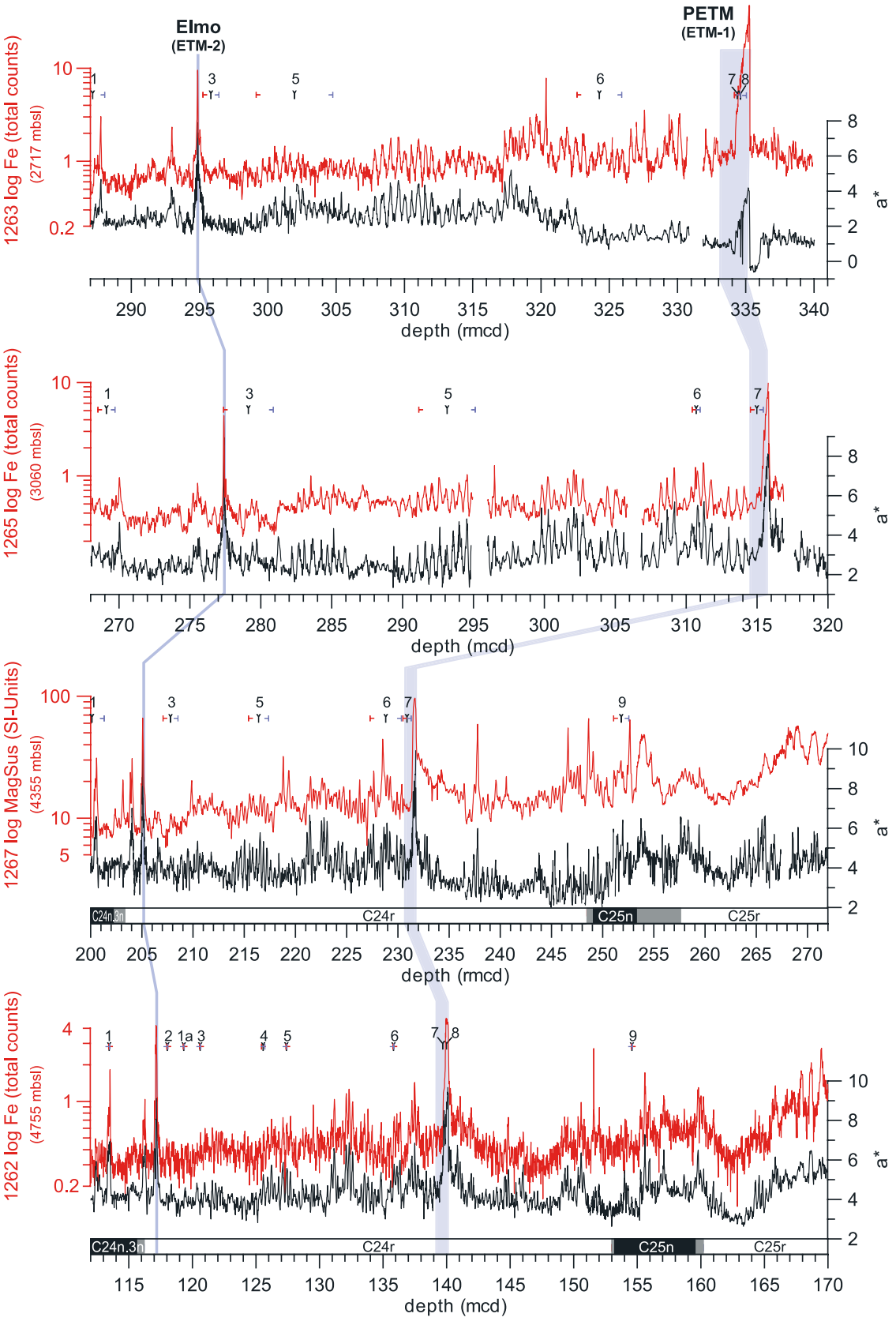
Elmo
(ETM-2)
PETM
(ETM-1)
1263 log Fe (total counts)
(2717 mbsl)
depth (rmcd)
1265 log Fe (total counts)
(3060 mbsl)
depth (mcd)
1267 log MagSus (SI-Units)
(4355 mbsl)
depth (rmcd)
1262 log Fe (total counts)
(4755 mbsl)
depth (mcd)
a*
C24n.3n
C24r
C25n
C25r

Figure 2

2.1. Physical Properties and X-Ray Fluorescence (XRF) Scanning

[6] Color reflectance data (L*, a*, b*), and whole core magnetic susceptibility data (MS) of the multisensor track (MS-MST) measurements were routinely measured during Leg 208 [*Shipboard Scientific Party*, 2004a]. Cyclic variations in these data reflect lithological changes at a decimeter to meter scale and served as the primary means for high-resolution correlation of Leg 208 sites [*Shipboard Scientific Party*, 2004b]. In this study, we preferred to use the a* value (red over green ratio, Figure 2) instead of the L* value because it revealed a much better signal for time series analysis.

[7] X-ray fluorescence (XRF) measurements of iron (Fe) show a significantly higher signal-to-noise ratio and a more consistent hole-to-hole agreement than any of the shipboard physical property measurements (e.g., GRA, color reflectance, MS). Therefore XRF data allow the construction of a more accurate high-resolution composite depth scale [*Evans et al.*, 2004; *Röhl and Abrams*, 2000]. For our study we measured the elemental composition of sediments from ODP Sites 1262, 1263 and 1265 at the Bremen ODP Core Repository (BCR) using the XRF core scanner II [*Röhl and Abrams*, 2000; *Röhl et al.*, 2000], which allows high-resolution, nearly continuous, nondestructive analyses of major and minor elements at the surface of split cores [*Jansen et al.*, 1998]. XRF data were collected every 2 cm down-core over a 1 cm^2 area using 30 s count time. We scanned along the shipboard composite depth section (mcd) of Sites 1262 (112–170 mcd) [*Shipboard Scientific Party*, 2004c], 1263 (287–340 rmcd) [*Shipboard Scientific Party*, 2004d], and 1265 (275–317 mcd) [*Shipboard Scientific Party*, 2004e] with overlapping sections at the splice tie points in order to check the accuracy of the shipboard splice.

2.2. Calcareous Nannofossil Biostratigraphy

[8] Upper Paleocene–lower Eocene calcareous nannofossil biohorizons across the magnetochrons C24r and C25n interval were identified at Site 1262. Biohorizons were defined from the distribution ranges of index species, obtained through semiquantitative counting of selected taxa. About 200 samples were collected at a resolution of one sample every 4–20 cm from Site 1262. These samples were processed following standard smear slide techniques, which were analyzed with a polarizing microscope, at ×1250 magnification. Semiquantitative data were obtained using analytical methods developed in previous studies [e.g., *Backman and Raffi*, 1997; *Backman and Shackleton*, 1983; *Rio et al.*, 1990], by counting the index species in a preselected area of the slide in which each field of view has a relatively constant particle (nannofossil) density. The abundance of each index species is converted to number/mm^2.

[9] The obtained abundance patterns are moderately affected by differential preservation of the nannofossil assemblages, in which both dissolution of susceptible species and overgrowth on resistant taxa, such as *Fasciculithus*, *Rhomboaster* and *Tribrachiatus*, were observed. The nannofossil assemblages showed the sequence of evolutionary changes that make up the biostratigraphic framework of the standard zonations of *Martini* [1971] and *Bukry* [1973, 1978], from NP8/NP9 (CP7/CP8) boundary to NP10/NP11 (CP9a/CP9b) boundary. We use "LO" (lowest occurrence) and "HO" (highest occurrence) to denote the first (lowest) and last (highest) occurrence of index species, respectively. Positions of the nannofossil biohorizons, as reported in Figure 2, are based on the new detailed data (at Site 1262 and PETM interval at Site 1263) and revised shipboard data (at Sites 1263, 1265 and 1267).

2.3. Magnetostratigraphy

[10] Discrete samples were taken from the working half cores of Sites 1262 and 1267 in 8 cm^3 cubes at 10 cm to 150 cm spacing. Dense sampling (up to 10 cm) was conducted over critical intervals such as the C24r-C24n reversal boundary. Samples were alternating field (AF) demagnetized in steps up to 40–60 mT, using the "double-demagnetization" technique [*Tauxe et al.*, 1995] for AF levels above 30 mT. A vertical drilling overprint was generally removed by 15 mT, and the remanence direction was calculated by principal component analysis [*Kirschvink*, 1980] for steps from 15 to 40 mT (4 to 6 points) for most samples. Directions with a maximum angular deviation [*Kirschvink*, 1980] >15° or samples that did not display univectoral decay during demagnetization were rejected. The remaining inclinations were used along with shipboard pass-through data to determine polarity. The position of the C24r/C24n reversal boundary at Site 1262 is taken from *Lourens et al.* [2005]. A summary table with the magnetostratigraphic interpretation of Sites 1262 and 1267 is available in the auxiliary material in Table S1.[1] The magnetostratigraphy for Site 1051 was taken from the revised interpretation of *Cramer et al.* [2003].

3. Results

3.1. XRF, Physical Properties, and Stratigraphy

[11] Physical property data and XRF-Fe intensity data (Tables S2, S3, and S4 in auxiliary material tables) in combination with magnetostratigraphic and biostratigraphic interpretation show that our studied interval comprises ~4.5 Ma at Sites 1262 and 1267, and about 2 Ma at Sites 1263 and 1265 (Figure 2). All four sites contain the PETM [*Zachos et al.*, 2005] and ETM2 [*Lourens et al.*, 2005] events, and exhibit extraordinary and explicit high-frequency cyclicity in the a*, MS, and Fe intensity records (Figure 2). The correlation between Fe intensity and a* values is high and is explained by the fact that a* is a measure of redness in the sediment, which largely reflects the concentration of iron (oxides) bearing minerals. Thus the observed variations in Fe concentration are interpreted to reflect the amount of terrigenous material in the sediment. Although, the MS record exhibits very similar patterns (i.e., high MS corresponds to high Fe intensity), the high-frequency variability seems less well amplified. The MS signal is smoothed by diamagnetic calcite and by postburial diagenetic alteration

[1] Auxiliary materials are available at www.pangaea.de (doi:10.1594/PANGAEA.603177).

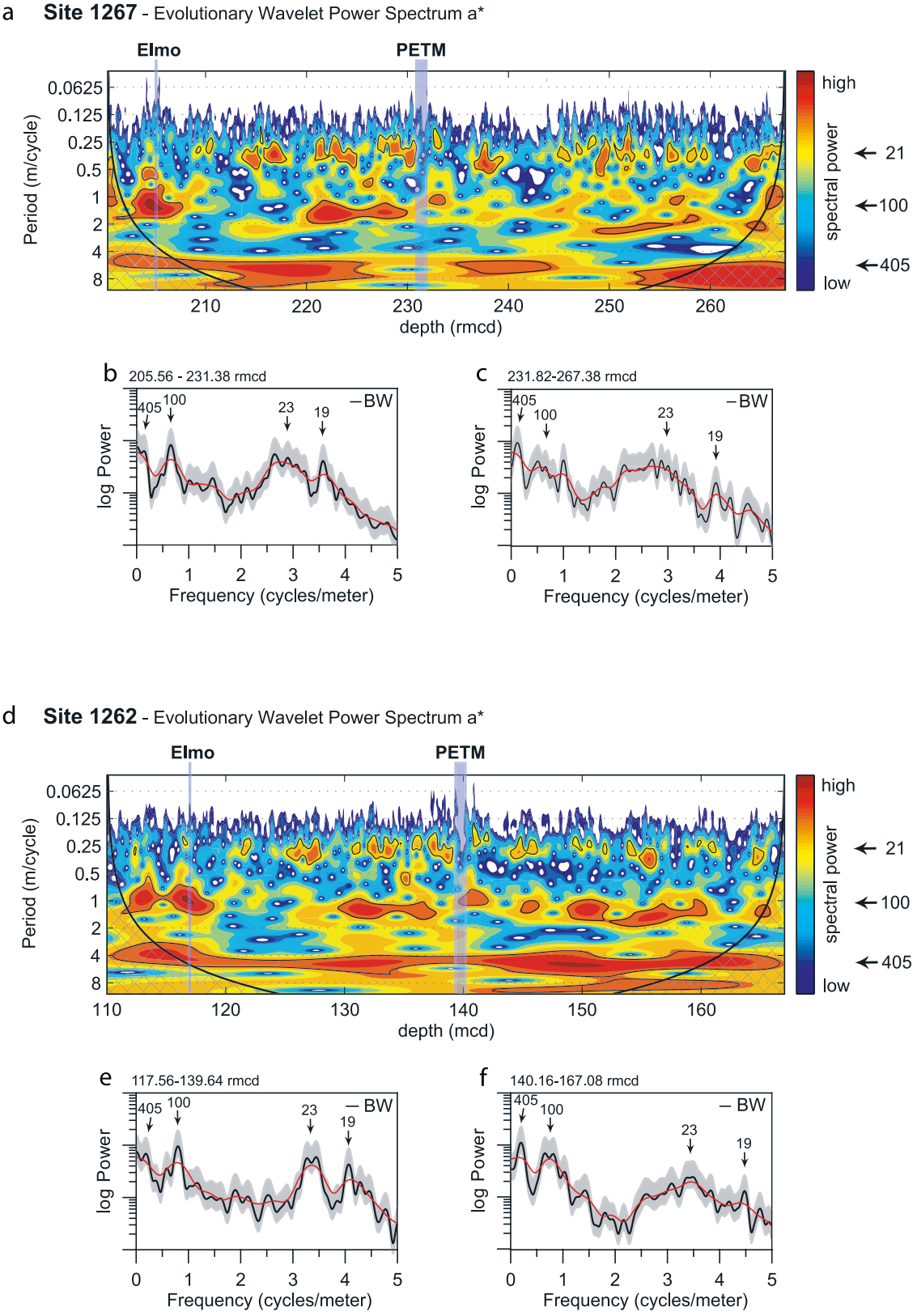
a Site 1267 - Evolutionary Wavelet Power Spectrum a*
Elmo
PETM
Period (m/cycle)
0.0625
0.125
0.25
0.5
1
2
4
8
210
220
230
240
250
260
depth (rmcd)
high
spectral power
low
21
100
405
b 205.56 - 231.38 rmcd
405
100
23
19
BW
log Power
Frequency (cycles/meter)
c 231.82-267.38 rmcd
d Site 1262 - Evolutionary Wavelet Power Spectrum a*
110
120
130
140
150
160
depth (mcd)
e 117.56-139.64 rmcd
f 140.16-167.08 rmcd

Figure 3

(redox changes of Fe). Because bulk iron concentration is less affected by postburial diagenetic alteration and analyzed at a much higher resolution we consider the Fe signal to be much more reliable.

[12] The prominent warming events are characterized by dark red to brown layers with all, very high a*, MS, and Fe values (Figure 2), caused by strong carbonate dissolution [*Lourens et al.*, 2005; *Zachos et al.*, 2005]. We established the best constrained biostratigraphy and magnetostratigraphy of the studied interval for the deepest Site 1262 (4755 m water depth). A magnetostratigraphy was also constructed for Site 1267, but the uncertainty in the position of the polarity boundaries is larger compared to Site 1262.

3.2. Revised Meters Composite Depth (rmcd) Scales

[13] A prerequisite for constructing a high-resolution cyclostratigraphy for the late Paleocene and early Eocene interval is a stratigraphically complete and undisturbed sequence. For this purpose, a composite depth section (or "splice") was constructed for each site during the leg using MS and color reflectance records with a 2.5 cm resolution. Here we evaluate and correct the shipboard composite depth (mcd) scales where needed by utilizing the new high-resolution Fe intensity data integrated with color data (a* values).

[14] This multiproxy comparison shows that the shipboard splice for Sites 1262 and 1265 are essentially correct, and thus suitable as a template for the other sites. We found through comparison with Site 1262 that Sites 1263 and 1267 shipboard splices required only minor revisions. Where needed, we vertically shifted the individual cores for each site without allowing expansion or contraction of the relative depth scale within any core, which is similar to the method of shipboard software "Splicer." We then assembled a new single spliced record of the revised composite depth section for Sites 1263 and 1267 avoiding intervals with significant disturbance or distortion. For the construction of the revised records, we mostly used the same tie points between holes as defined for the shipboard splice. Changes in the position of tie points in the new revised spliced record (compared to the shipboard splice) are highlighted as bold letters in the splice tables of each site.

[15] The shipboard splice for Site 1263 is relatively robust down to 296 mcd, where the first adjustment, only 8 cm, was made. Below 318.50 mcd we identified a larger mismatch of Core 1263B-27X to cores of Holes A, C, and D, which was likely the result of differential stretching of APC and XCB cores [*Shipboard Scientific Party*, 2004d]. We assembled a new composite record (rmcd) for Site 1263 to match the record from Site 1262 (Tables S5 and S6 in the database). The Site 1267 splice (Tables S7 and S8 in the database) needed minor refinements only in order to optimize the spliced record down to centimeter-scale cycles. We therefore decided to construct a modified splice below 180.25 mcd to also match the Site 1262 record.

4. Cyclostratigraphy

4.1. Cycles in the Depth Domain

[16] To investigate whether the cyclicity in our data records is related to orbital forcing we essentially followed the approach of *Weedon* [1993, 2003] and calculated evolutionary spectra in the depth domain to both identify the dominant cycle periods, and to detect distinct changes in these cycle periods. Wavelet analysis was used to compute evolutionary spectra. Wavelet software was provided by C. Torrence and G. Compo, and is available at http://paos.colorado.edu/research/wavelets. Prior to wavelet analysis the data were detrended and normalized.

[17] The presence of parallel bands in the wavelets for Sites 1267 and 1262 demonstrate that spectral power is confined to distinct frequency bands (Figure 3). The absence of a strong shift in the bands for both sites suggests stable and uniform sedimentation rates prevailed throughout the investigated interval. A slight shift toward lower periods from 150 to 140 mcd in the evolutionary spectra for Site 1262 might indicate a decrease in sedimentation rate prior to the PETM (~140 mcd) (Figure 3). Spectral analyses of the interval prior to the PETM (Figure 3c for Site 1267, Figure 3f for Site 1262), and between PETM and ETM2 (Figure 3b for Site 1267, Figure 3e for Site 1262) reveal related frequencies of the dominant cycles: Site 1267 shows dominant cycles at 0.15, 0.66, and 2.6–3.6 m/cycle with a minor shift at high frequencies across the PETM. Site 1262 exhibits dominant cycles at 0.13, 0.66, and 2.6–4.1 m/cycle. The periodicities have a nearly perfect 1:4:20 frequency ratio and are diagnostic for a combination of the long (405 kyr) and short (100 kyr) eccentricity cycle, and the mean precession (21 kyr) cycle. Spectral analysis of Site 1262 also reveals the split precession (23.7 kyr, 22.4 kyr, and 19 kyr), and split short eccentricity (125 kyr and 95 kyr)

Figure 3. Evolutionary wavelet analysis of the a* value for (a) Site 1267 with power spectra for periods (b) between the PETM and Elmo horizon and (c) prior to the PETM and (d) Site 1262 in the depth domain with power spectra for periods (e) between the PETM and Elmo horizon and (f) prior to the PETM. The shaded contours are normalized linear variances, with blue representing low spectral power and red representing high spectral power. The black contour lines enclose regions of greater than 95% confidence. Cross-hatched regions on either end indicate the cone of influence where edge effects become important. Note the distinct bands (marked by arrows) that run across the spectra that indicate the dominance of Milankovitch-related periods (precession with a central frequency of 21 kyr and eccentricity with frequencies at 100 and 405 kyr). In Figures 3b and 3c and 3e and 3f the Blackman-Tukey power spectra (bold black line) have been calculated by the AnalySeries program [*Paillard et al.*, 1996] using 80% confidence interval (gray area, 30% of series); bold red line is the estimated background noise (10% of series). Bandwidth (BW) and confidence limits are based on a Bartlett window with a number of lags that equal 30% of the length of the data series. The spectra reveal strong spectral peaks at precession and eccentricity-related periodicities according to biostratigraphy and magnetostratigraphy.

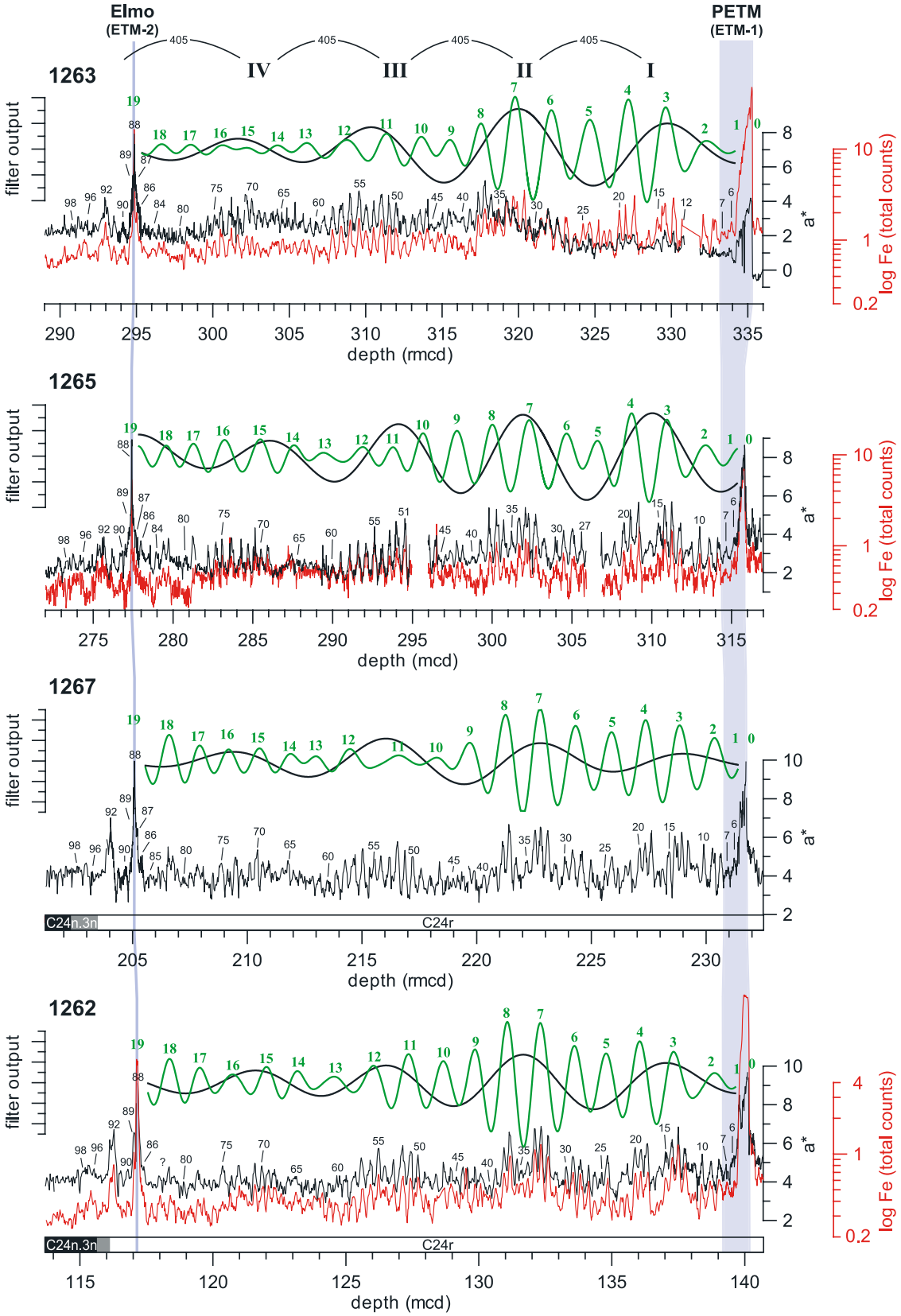
Elmo
(ETM-2)
PETM
(ETM-1)
405
IV
III
II
I
1263
filter output
a*
log Fe (total counts)
depth (rmcd)
1265
depth (mcd)
1267
C24n.3n
C24r
depth (rmcd)
1262
depth (mcd)

Figure 4

related peaks. This is compelling evidence for a unique match of the sedimentary rhythm to orbital forcing as proposed by *Herbert et al.* [1995]. The magnetostratigraphic data likewise suggest that these dominant cycles correspond to variations in Earth's eccentricity and precession. The most important result is the evidence of the long eccentricity cycle, because the long duration of stability of the 405-kyr eccentricity cycle can be used for orbital tuning [*Laskar et al.*, 2004; *Varadi et al.*, 2003]. The individual spectra of a* and Fe do not show indication for obliquity-related cyclicity.

4.2. Cyclostratigraphy From the PETM to the Chron C24r/C24n Boundary

[18] We used direct cycle counting and Gaussian band-pass filtering of the data to construct a cyclostratigraphy from the PETM to the chron C24r/C24n boundary using data from Sites 1262, 1263, 1265, and 1267 (Figure 4a). For the band-pass filtering we removed the PETM and the Elmo horizon from the data in order to avoid filter disturbance. As a fixed starting point to count precession cycles we used the onset of the carbon isotope excursion (CIE) [*Zachos et al.*, 2005], which is a global event [*Kennett and Stott*, 1991; *Schmitz et al.*, 2001] that defines the Paleocene-Eocene boundary [*Luterbacher et al.*, 2000]. For counting toward the younger section from the PETM we assigned positive numbers (i.e., for precession cycles, P_{10}; for short eccentricity cycles, E_{10}), counting back in time older than the PETM we used negative numbers (i.e., P_{-10}; E_{-10}). The most expanded succession of the PETM was recovered at Site 1263; but all Leg 208 sites are condensed during the PETM because of dissolution of calcium carbonate [*Zachos et al.*, 2005]. In addition, the PETM interval at Walvis Ridge does not reflect obvious sediment cycles but according to the cycle counting at Site 690 the duration of the period of the clay layer with low calcium carbonate content at Walvis Ridge covers the equivalent of 5 precession cycles ($\sim$105 kyr). The duration of the interval with lower carbonate values at Site 690 from cycle counting [*Röhl et al.*, 2000] is consistent with the He isotope age model of *Farley and Eltgroth* [2003]. For the Walvis Ridge sites we labeled the first precession cycle after the clay layer, starting with the recovery interval of the PETM, as precession cycle 6 (Figure 4a). On the basis of on this, from the base of the CIE we counted 88 precession cycles up to the ETM2 (Figure 4a). Cycle counting was straightforward from P cycles P_6 to P_{85}. Minor gaps at Sites 1263 and 1265 (Figure 4a) are covered by records from Sites 1262 and 1267. In the area of cycles P_{86} to P_{90} counting was difficult at the deeper Sites 1262 and 1267 because of the carbonate dissolution within the Elmo horizon [*Lourens et al.*, 2005]. However, both Sites 1265 and 1263 indeed exhibit well pronounced cycles numbered 86 to 88 (Figure S1 in auxiliary material). The ETM2 reveals similar features as the PETM with stronger condensation of sections at deeper sites [*Lourens et al.*, 2005]. The succession above the Elmo horizon exposes clear cyclicity at least up to cycle P_{98}, which is well within chron C24n.3n as pinpointed in Sites 1262 and 1267. The best constrained paleomagnetic signal retrieved from Site 1262 shows that the C25r/C24n boundary is close to cycle P_{96} with an uncertainty of $\sim$2 cycles.

[19] After the extraction of the short- and long-term related eccentricity cycles from the a* record at all four sites (Figure 4a) 17 short eccentricity cycles are identified that encompass the precession-related cycles P_7 to P_{85}. Each short eccentricity cycle consists therefore of $\sim$4.5 precession-related sedimentary cycles. Application of this relationship would imply that cycles P_{-3} to P_6 represent two full eccentricity cycles. In addition, cycles P_{85} to P_{90} compose one short-term eccentricity cycle that accompanies the ETM2. Accordingly, the ETM2 coincides with short-term eccentricity maximum E_{19}, and the onset of the PETM with short-term eccentricity maximum E_0. Moreover, the records reveal $\sim$4.5 long-term eccentricity cycles between the onset of the PETM and ETM2.

4.3. Cyclostratigraphy From Below the Chron C25r/C25n Boundary to the PETM

[20] Direct cycle counting and Gaussian band-pass filtering of data from Sites 1262 and 1267 has been used to construct a cyclostratigraphy from below the C25r/C25n reversal boundary to the PETM (Figure 4b). A total of 105 precession-related cycles were identified for this interval. Cycle counting is straightforward for Site 1262 and 1267, although the a* signal in Site 1267 is noisy between 245 and 257 rmcd, because of drilling disturbance [*Shipboard Scientific Party*, 2004f]. As check on the cycle counts, we compared our records of Sites 1262 and 1267 with the Fe intensity data from ODP Site 1051 [*Röhl et al.*, 2003]. This comparison shows that 5 precession-related cycles are

Figure 4. Cycle counting of (a) early Eocene and (b) late Paleocene sediments at Walvis Ridge using the a* value (black line) of the color data and high-resolution Fe intensity data (Sites 1262, 1265, and 1267, red line). In Figure 4b, Fe data from Site 1051 [*Röhl et al.*, 2003] versus a new composite depth (rmcd, this study) are plotted. For each site the small black numbers indicate the number of precession cycles relative to the onset of the PETM. The position of the PETM and the Elmo horizon are indicated (blue line) and are thus according to the precession cycle counting 88 cycles apart. The short (bold green) and long (bold black) eccentricity-related cycles have been extracted by Gaussian filtering of a* value (Sites 1267 and 1265) and Fe intensity data (Sites 1262 and 1263). For Site 1262, filter frequency for long (short) eccentricity cycle is 0.19 ± 0.057 (0.80 ± 0.24) cycles/m. For Site 1267, filter frequency for long (short) eccentricity cycle is 0.15 ± 0.045 (0.66 ± 0.20) cycles/m. For Site 1263, filter frequency for long (short) eccentricity cycle is 0.10 ± 0.03 (0.41 ± 0.123) cycles/m. For Site 1265 filter frequency for long (short) eccentricity cycle is 0.12 ± 0.036 (0.46 ± 0.138) cycles/m. The green numbers indicate the short eccentricity maxima, whereas cycle E_0 comprises the PETM, thus the distance between the PETM and Elmo horizon is 19 short eccentricity cycles. In addition, we labeled the long eccentricity maxima with roman numbers -V to IV relative to the PETM.

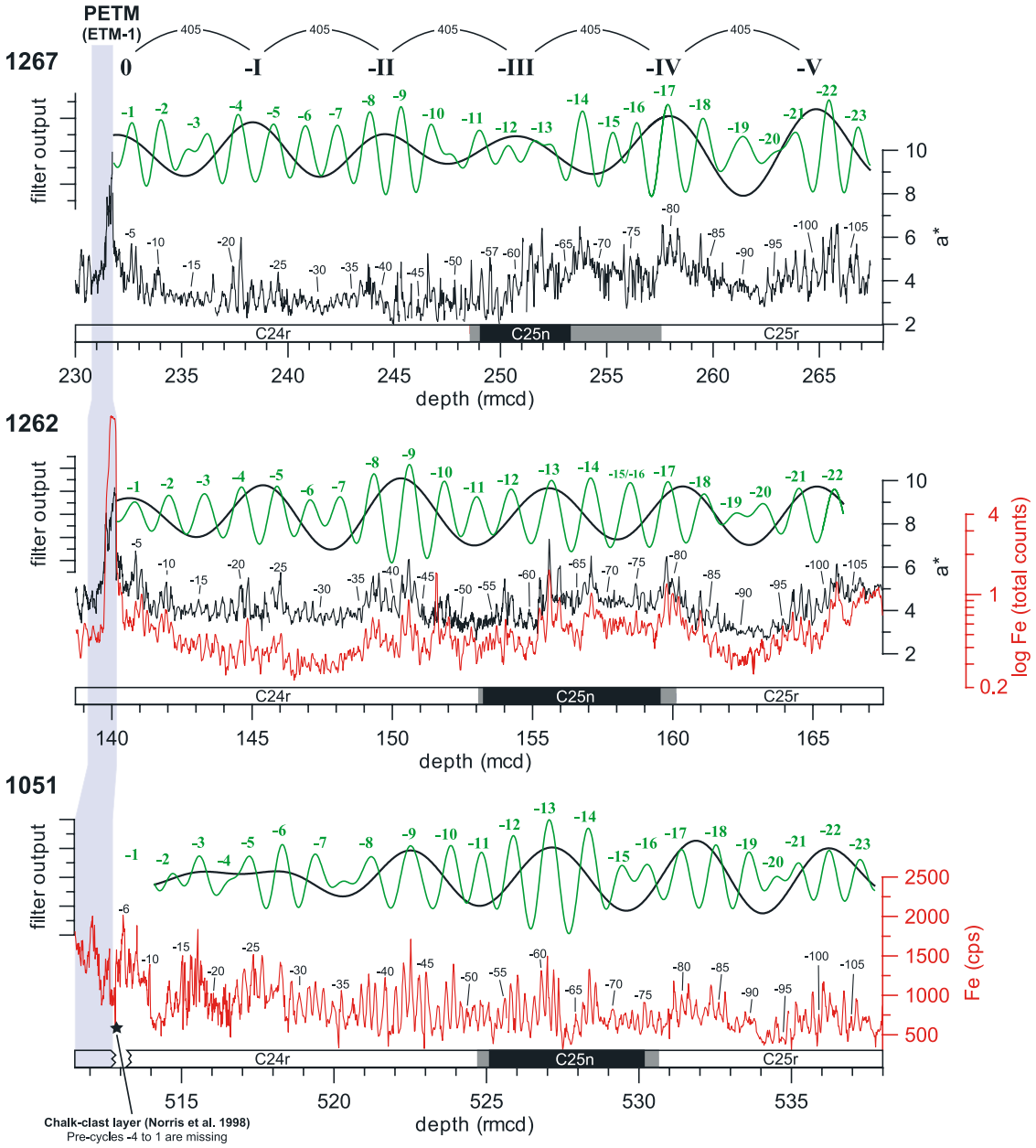

Figure 4. (continued)

missing at Site 1051 (P_{-4} to P_1) between cycles P_{-6} and the onset of the PETM. This might imply that a debris flow of chalk clasts observed just below the CIE [*Katz et al.*, 1999; *Norris et al.*, 1998] may have eroded ~125 kyr of sediment at Site 1051 rather than the previously estimated several ten thousand years [*Norris and Röhl*, 1999]. Our revised meters composite section (rmcd) for Site 1051 also results into the identification of 3 additional precession-related cycles in the interval from 515 to 517 rmcd. The well pronounced cyclicity at Site 1051 between cycles P_{-30} and P_{-80} substantially helped to constrain the correct number of precession cycles across chron C25n. The depth filter output (Figure 4b) resulted in 23 short (including the short eccentricity cycle E_0 that encompasses the PETM), and 5.5 long eccentricity cycles from the PETM to cycle P_{-105}. A closer look at the filter outputs for each site (Figure 4b) shows differences at short eccentricity cycles E_{-3} and $E_{-15/-16}$. However, combining the data from different sites we feel confident that E_{-3} represents only one cycle, and that E_{-15} and E_{-16} are separate cycles as indicated by the filter output of Sites 1267 and 1051. These uncertainties are bound to intervals in the different records characterized by low-amplitude variations, which might affect the filter output. The characteristic precession-related cycle patterns of the three sites from two different areas in the Atlantic Ocean enables us however to establish a very

Table 1. Estimates for the Duration of Magnetochrons and the Position of Eocene Events Based on Cycle Counting[a]

Site(s)	Study	Eccentricity Cycles	Precession Cycles	Duration, kyr
		C24r		
577, 550, 1051, 690	*Cramer et al.* [2003]	~24		~2350 ± 100
1051A	*Cramer* [2001]		115–157	2856 ± 441
1051	*Röhl et al.* [2003]		137	2877
1051	this study		146 ± 5	3066 ± 105
1262	this study		148.5 ± 2.5	3118.5 ± 52.5
1267	this study		154 ± 6	3234 ± 126
1051, 1262, 1267	this study		148	3108
spline	*Cande and Kent* [1995]			2557
spline	GTS2004			2858
		C25n		
577, 550, 1051, 690	*Cramer et al.* [2003]			~450
1051	*Röhl et al.* [2003]		24 ± 1	504 ± 21
Zumaia	*Dinarès-Turell et al.* [2002]		22 ± 1	462 ± 21
1262	this study		24 ± 1	504 ± 21
1267	this study		(12 ± 14)	(252 ± 294)
1051, 1262	this study		23	483
spline	*Cande and Kent* [1995]			487
spline	GTS2004			515
		Base C24r to PETM (base of CIE)		
577, 550, 1051, 690	*Cramer et al.* [2003]		~39–41	850 ± 30
1051A	*Cramer* [2001]		43 ± 2	903 ± 42
1051	*Röhl et al.* [2003]		45 ± 1	945 ± 21
Zumaia	*Dinarès-Turell et al.* [2002]		47	987
1262	this study		53 ± 1	1113 ± 21
1267	this study		55 ± 2	1155 ± 42
1051	this study		53 ± 2	1113 ± 42
1051, 1262, 1267	this study		53	1113
spline	*Cande and Kent* [1995]			904
spline	GTS2004			865
		Base C24n to PETM (Base of CIE)		
577, 550, 1051, 690	*Cramer et al.* [2003]			~1500
1051A	*Cramer* [2001]		93 ± 19	1953 ± 399
1051	*Röhl et al.* [2003]		92	1932
1262	this study		95 ± 2	1995 ± 42
1267	this study		99 ± 4	2079 ± 84
1051	this study		93 ± 3	1953 ± 63
1051, 1262, 1267	this study		95	1995
spline	*Cande and Kent* [1995]			1653
spline	GTS2004			1992
		Base C24n to Elmo		
1262	this study		8 ± 2	168 ± 42
1267	this study		11 ± 4	231 ± 84
1262, 1267	this study		8	168
		ELMO to PETM		
577, 550, 1051, 690	*Cramer et al.* [2003]			1320 ± 30
1262, 1267	*Lourens et al.* [2005]	~21	-	2035
1262, 1263, 1265, 1267	this study	19	87 ± 1/2	1827 ± 11

[a]Errors take into account only the uncertainty of the exact position of magnetic reversal boundaries at 1051, 1262, and 1267; the error associated with cycle counting is not added.

accurate cyclostratigraphy which we consider to be reliable within one precession cycle.

5. Discussion

[21] To construct a timescale for the early Eocene warming events, and their relative position to paleomagnetic boundaries and biozones we follow the metronome approach of *Herbert et al.* [1995] assuming that each cycle represents a duration equal to the mean period of the orbital parameter that forced its formation. According to *Herbert et al.* [1995] 21-kyr is a good estimate for the mean of the main modern precession periods for cycle counts of more than ~7 cycles. Previous studies have shown that the main periodicities of precession and obliquity have increased with time because of tidal friction resulting from the gravitational attraction of the sun and moon [e.g., *Berger et al.*, 1992; *Dehant et al.*, 1987; *Hinnov*, 2000; *Laskar*,

Table 2. Revised Estimates for Calcareous Nannoplankton Biostratigraphic Datum Levels at Site 1262 Relative to the Age of the PETM[a]

Event	Nannofossil Marker	Mean Depth, mcd	Mean Age Relative to Onset PETM, kyr	Chron Percentage From Top[b]
HO	*T. contortus*	118.085 ± 0.105	1740 ± 8	C24r.082
Decrease	*D. multiradiatus*	119.375 ± 0.105	1646 ± 7	C24r.112
LO	*T. orthostylus*	120.665 ± 0.105	1558 ± 7	C24r.140
LO	*T. contortus*	125.615 ± 0.015	1177 ± 1	C24r.263
LO	*D. diastypus*	127.445 ± 0.105	1054 ± 7	C24r.302
HO	*Fasciculithus spp.*	135.865 ± 0.105	403 ± 9	C24r.511
HO	*R. calcitrapa gr.*	139.715 ± 0.005	85 ± 1	C24r.613
Abundance crossover	*Fasculiths/Z. bijugatus*	139.78 ± 0.01	74 ± 2	C24r.616
Lowermost specimen	*T. bramlettei*	139.975 ± 0.005	36 ± 1	C24r.628
LO	*R. calcitrapa gr.*	140.015 ± 0.005	27 ± 1	C24r.631
Decrease in diversity of	*Fasciculithus*	140.1475 ± 0.0025	−5 ± 1	C24r.642
LO	*D. multiradiatus*	154.605 ± 0.105	−1238 ± 7	C25n.226
HO	*Ericsonia robusta*	157.995 ± 0.105	−1500 ± 11	C25n.739

[a]Abbreviations are HO, Highest Occurence; LO, Lowest Occurence; minus sign indicates before PETM. Error takes into account only the sampling distance; error associated with cycle counting is not added.
[b]Read, for example, C24r.082 as 8.2% of chron 24r follows the biostratigraphic level.

1999; *Laskar et al.*, 2004; *Néron de Surgy and Laskar*, 1997]. Although 55 Ma ago the average precession frequency is predicted to have been higher than today (∼1/(20.7 kyr) [*Berger et al.*, 1992]) because the Earth-Moon distance was shorter, and the rotation of the Earth faster [*Laskar et al.*, 2004], we used 21 kyr as the mean duration for the counted precession cycles because of the close correspondence between the ratios of modern eccentricity and precession cycles with those observed in this study. Additionally, this allowed for a more direct comparison with former estimates based on cycle counting [*Cramer*, 2001; *Röhl et al.*, 2003]. Because we counted more than 200 precession cycles the estimated timescale error by using orbital-forced cycle stratigraphy is less than 2% [*Hinnov*, 2004].

5.1. Duration of Chrons C24r and C25n

[22] Chron C24r consists of 148.5 ± 2.5 precession cycles according to our cycle counting and the geomagnetic polarity data for Site 1262, which corresponds with a duration of 3118.5 ± 52.5 kyr (Table 1). A total of 154 ± 6 precession cycles (3234 ± 126 kyr) have been counted at Site 1267, because of the weakly defined top of C24r. Reanalysis of Site 1051 revealed 8 additional precession cycles over the previous counts which were considered to provide "minimum" estimates [*Cramer et al.*, 2003; *Ogg and Bardot*, 2001; *Röhl et al.*, 2003], resulting in a total of 146 ± 5 precession cycles (or 3066 ± 105 kyr). On average, C24r has a mean duration of ∼3108 kyr, but we consider the estimate on Site 1262 (3118 ± 52 kyr) to be the most reliable (Table S1). This estimate is 260 kyr larger than that presented in the GTS2004 [*Gradstein et al.*, 2004] (see discussion below) which was based on the minimum cycle counting of *Röhl et al.* [2003]. Discrepancies with previous cyclostratigraphies and timescales [*Cramer*, 2001; *Cramer et al.*, 2003; *Ogg and Smith*, 2004; *Röhl et al.*, 2003] can be attributed to unrecognized gaps in previously single-cored sites as well as poorly expressed lithological cycles resulting in underestimates of cycles and the durations of specific intervals.

[23] In contrast to magnetochron C24r, the duration of chron C25n is well constrained in both marine- and land-based sections [e.g., *Dinarès-Turell et al.*, 2002; *Röhl et al.*, 2003]. Cycle counting in the record from Site 1262 yields 24 ± 1 (504 ± 21 kyr) precession cycles within chron C25n (Table 1). The top of C25n is well defined in Site 1267, but not its base. Therefore just part of C25n (12 ± 14 precession cycles, = 252 ± 294 kyr) is represented in the Site 1267 record. The duration of C25n as determined at Site 1262, is similar to the estimate for Site 1051 (Figure 4b). Combining the cycle count for both Sites 1262 and 1051 yields an average of 23 precession cycles (or duration of 483 kyr) for chron C25n. This agrees very well with previous estimates from Site 1051 [*Röhl et al.*, 2003] and the land-based Zumaia section [*Dinarès-Turell et al.*, 2002] (Table 1).

5.2. Calcareous Nannofossil Biochronology

[24] The lowest occurrence (LO) of *Tribrachiatus bramlettei* was chosen by *Martini* [1971] to define the base of the calcareous nannofossil zone NP10, which often was used as an approximation of the P/E Boundary. The identity and systematic position of nannofossil marker species in C24r has been discussed by various authors, and their different viewpoints have lead to different interpretations of the same data [see, e.g., *Aubry et al.*, 1996; *Berggren and Aubry*, 1996; *Cramer et al.*, 2003; *Raffi et al.*, 2005]. For example, the unreliability (diachrony) of *T. bramlettei* LO biohorizon [e.g., *Cramer et al.*, 2003; *Raffi et al.*, 2005] suggests to consider the LO of *Rhomboaster calcitrapa* gr. (= LO of *Rhomboaster* spp.), which defines the base of *Bukry*'s [1973, 1978] subzone CP8b and occurs within the CIE interval, a better biohorizon to approximate the boundary. Moreover, recent results from Leg 199 indicate that the previously proposed subdivision of *Martini*'s [1971] zone NP10 (NP10a–NP10d) [*Aubry*, 1999] is erroneous, because of differences in stratigraphic relationship between the index species *Tribrachiatus contortus* and *Tribrachiatus digitalis* [*Raffi et al.*, 2005]. This finding is confirmed by the results at Site 1262. Because of the needed extensive revision of the late Paleocene and early Eocene biostratig-

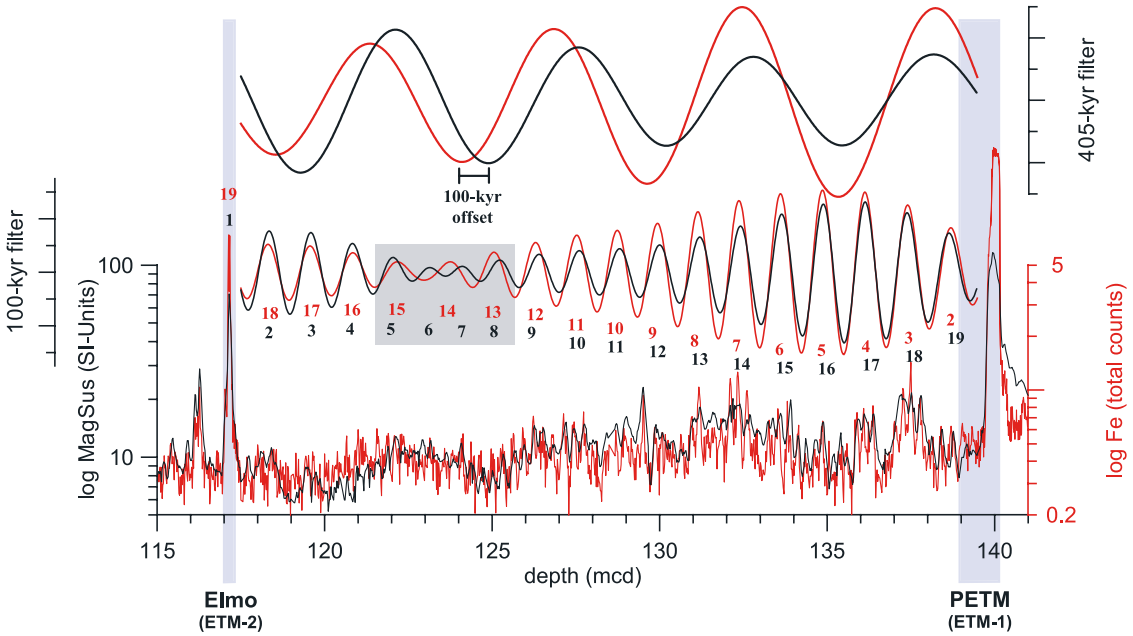

Figure 5. Comparison of filter outputs derived from Site 1262 magnetic susceptibility (MS) (black) and Fe intensities (red) between the PETM and Elmo horizon. The same Gaussian filters were applied to extract the 100-kyr component (0.8 ± 0.104 cycles per m) and the 405-kyr component (0.17 ± 0.022 cycles per m) as done by *Lourens et al.* [2005] to show how the resolution and quality of data have an influence on the filter output. The black numbers represent the number of short eccentricity cycles as proposed by *Lourens et al.* [2005], whereas the red numbers represent the number of short eccentricity cycles as proposed in this study. The gray box highlights the interval where the filter outputs between MS and Fe intensity give inconsistent results. The resulting mismatch of ~100 kyr between the two data sets is also present as an offset in the long eccentricity filter output.

raphy, we here provide information on the relative position of nannofossil events in C24r and 25n as well as their absolute age only (Table 2).

5.3. Relative Timing of Early Eocene Warming Events

[25] The pronounced precession cycles within C24r allowed us to define the exact positions of both early Eocene hyperthermal events, the PETM and ETM2 [*Kennett and Stott*, 1991; *Lourens et al.*, 2005]. For the PETM we defined the onset (P_0) as a fixed point, and for the position of ETM2 we chose to use the associated maximum peak in a* values (P_{88}) as a fixed point (= midpoint Elmo horizon). According to our cyclostratigraphy the onset of the PETM is 53 ± 1 (1113 ± 21 kyr) and 55 ± 2 (1155 ± 42 kyr) precession cycles above the C25n/C24r reversal boundary in the Sites 1262 and 1267 records, respectively. The combination of Walvis Ridge sites and Site 1051 yields 53 ± 2 (1113 ± 42 kyr) cycles between the PETM and C25n/C24r (Table 1). This new estimate of 53 precession cycles representing 1113 kyr is ~160 kyr longer than previous estimates from marine-based sections [*Cramer*, 2001; *Cramer et al.*, 2003; *Röhl et al.*, 2003]. These latter estimates were based, however, on the incomplete Site 1051 only, which also contains a slumped interval at the base of the PETM [*Katz et al.*, 1999]. Other records (e.g., DSDP Sites 550, 577, and ODP Site 690) clearly possess gaps because of stratigraphic hiatuses or recovery issues [*Cramer et al.*, 2003]. In contrast, a total of only 47 precession cycles have been counted in the Zumaia section between the base of C24r and the PETM [*Dinarès-Turell et al.*, 2002]. The discrepancy with our estimate is likely the result of one or a combination of factors including; (1) the missing interval from −12 to −14 m in the Zumaia outcrop [*Dinarès-Turell et al.*, 2002], (2) less developed precession cycles (overhanging carbonate banks), and/or (3) the duration of the thick clay interval associated with base of PETM.

[26] In the interval between the PETM and the C24r/C24n reversal boundary we identified 95 ± 2 (1995 ± 42 kyr), 99 ± 4 (2079 ± 84 kyr), and 93 ± 3 precession cycles (1953 ± 63 kyr) for Sites 1262, 1267 and 1051, respectively (Table 1). On the basis of correlation of the three sites we assigned 95 precession cycles (or 1995 kyr) from the PETM to the top of C24r. The difference between our results and those of *Röhl et al.* [2003] for Site 1051 can be largely explained by the adoption of the new high-resolution paleomagnetic data of *Cramer et al.* [2003]. Our results show, moreover that the interval between the onset of the PETM and the ETM2 spans 87 ± 0.5 precession cycles (1827 ± 11 kyr). This time span is equivalent to ~19 short eccentricity cycles. Previously, *Lourens et al.* [2005] estimated 21 short eccentricity cycles for this interval based on the recognition of 18 short eccentricity cycles in the MS and L* records of Sites 1262

and 1267 between the top of the PETM and the base of the Elmo horizon (Figure 5), and the assumption that the PETM consists of 11 precession cycles [*Röhl et al.*, 2000]. They concluded that both the ETM2 and the onset of the PETM are related to maxima of the 405-kyr eccentricity cycle. Spectral analysis of the higher-resolving and higher-quality data presented in this study, however, reveal only 17 short eccentricity cycles between the top of the PETM and the base of the Elmo horizon now (Figure 4). Using the same band-pass filter as given by *Lourens et al.* [2005] (see auxiliary material Figure S1) the series for Fe (and a*) of Site 1262 reveals one short eccentricity cycle less than that of the MS in the interval of low-amplitude variability around 125 mcd (Figure 5). If we consider the quality (signal-to-noise ratio) of the MS and L* data subordinate to that of the Fe and a* records, this implies that *Lourens et al.* [2005] overestimated the amount of short-term eccentricity cycles in this interval. Because of the consistency between precession cycle counting and band-pass filtering of proposed short eccentricity cycles in our records, we conclude that the distance between the top of the PETM and the base of the Elmo horizon spans 17 rather than 18 short eccentricity cycles.

[27] Secondly, applying the He isotope age model [*Farley and Eltgroth*, 2003] proposes a much shorter duration (about 90–140 kyr) than the 11 precession cycles assumed for the duration of the PETM [*Röhl et al.*, 2000], even though this method also includes many uncertainties in particular for the recovery interval of the PETM [*Farley and Eltgroth*, 2003]. Derived from the detailed correlation of Walvis Ridge Fe data to those of Site 690 in the Southern Ocean [*Zachos et al.*, 2005], the interval from the onset of the PETM to the base of eccentricity cycle 19 of *Lourens et al.* [2005] could alternatively be made up of about 7 to 8 rather than 11 precession cycles. As a consequence, our new results suggest that both the PETM and ETM2 may correspond to short-term eccentricity maxima, but in contrast to previously thought [*Lourens et al.*, 2005], both events are not exactly tied to maxima in the long-term eccentricity (405 kyr) cycle, because they are exactly 4.5 long-term eccentricity cycles apart.

[28] Finally, we summarized the relative position of the PETM and ETM2 within C24r following the system of *Hallam et al.* [1985] and the recommendation of *Cande and Kent* [1992] to use an inverted stratigraphic placement relative to the present. We propose that the duration of chron 24r is 3118 kyr (148 precession cycles) and that the onset of the PETM is 1995 kyr (95 precession cycles) before the chron C24r/C24n boundary. As such, the notation of C24r.64 is assigned to the onset of the PETM indicating that 64% of chron C24r follows the onset of the PETM. Similarly, a compilation of continental sections from the Bighorn Basin yields exactly the same relative stratigraphic position with respect to the chron C24r/C24n boundary [*Wing et al.*, 2000]. The ETM2 is located 8 ± 2 precession cycles or 168 ± 42 kyr at Site 1262 and 11 ± 4 precession cycles or 231 ± 84 kyr at Site 1267 below the chron C24r/C24n boundary. We considered the results from Site 1262 to be more reliable because of the higher quality in paleomagnetic data. Following the same stratigraphic concept, the ETM2 is labeled C24r.05 indication that 5% of chron C24r follows the event.

5.4. Toward an Absolute Timescale for the Late Paleocene and Early Eocene

[29] The records from the Walvis Ridge display a strong precession signal, which theoretically could be used for orbital tuning in a similar manner to the tuning of the Oligocene and Miocene at the Ceara Rise [*Shackleton and Crowhurst*, 1997; *Shackleton et al.*, 1999, 1995]. A direct tuning of the late Paleocene to early Eocene records to astronomical solutions is hampered because of the limited precision of the orbital solution [*Laskar et al.*, 2004; *Varadi et al.*, 2003]. In fact, the orbital solution of *Laskar et al.* [2004] (La2004) is considered to be valid back to 40 Ma [*Pälike et al.*, 2004]. The imprecise knowledge of the solar oblateness term J_2 is one of the main sources of uncertainty in the La2004 solution [*Laskar et al.*, 2004]. This limits an accurate age determination of successive minima in the very long eccentricity cycle (~2.4 Ma), which is the prerequisite to set up a first-order timescale [*Hilgen*, 1991; *Pälike et al.*, 2004; *Shackleton et al.*, 2000] in the Paleogene. Another eccentricity time series, solution R7 of *Varadi et al.* [2003] (Va2003), is very similar to La2004 back to ca. 45 Ma, but diverges beyond that age for the same reason. As a consequence, *Laskar et al.* [2004] recommended that for the construction of an astronomically calibrated timescale in the Paleogene only the very stable 405-kyr-long eccentricity period should be utilized. The period is related to the leading g2-g5 argument in the orbital solution of eccentricity, which has an age uncertainty of about 20 kyr at 50 Ma [*Laskar et al.*, 2004]. Nevertheless, in the following section we will make a tentative comparison between our records and the La2004 and Va2003 solutions to give new insight into currently used absolute age models.

[30] An effective method to assess the relationship between amplitude modulation in the data and in the hypothetical forcing is complex demodulation [*Shackleton et al.*, 1995]. In order to compare our data with current astronomical solutions we first have to extract the short and stable long eccentricity modulation from the climatic precession signal encoded in the data. We extracted the amplitude modulation of the climatic precession (~21 kyr) and the main orbital eccentricity signal (~405 kyr, ~100 kyr) of the data using the freeware ENVELOPE [*Schulz et al.*, 1999]. ENVELOPE estimates temporal changes in the signal amplitude of unevenly spaced data at a given period using a modified version of the harmonic-filtering algorithm of *Ferraz-Mello* [1981]. To obtain a comparable relative timescale for our records we used the cycle counting age model assuming ~21 kyr for the precession cycle duration and arbitrarily set an age of 1 Ma for the Elmo horizon. The resulting time series and sedimentation rates for the Fe intensity data from Site 1262 are plotted in Figure 6a. The age model is provided in auxiliary material Table S9. The average sedimentation is 1.2 cm/kyr, though rates seem to vary in a cyclical fashion with lower rates corresponding with the low-carbonate intervals, possibly because of dissolution. Likewise, the PETM and Elmo horizon are char-

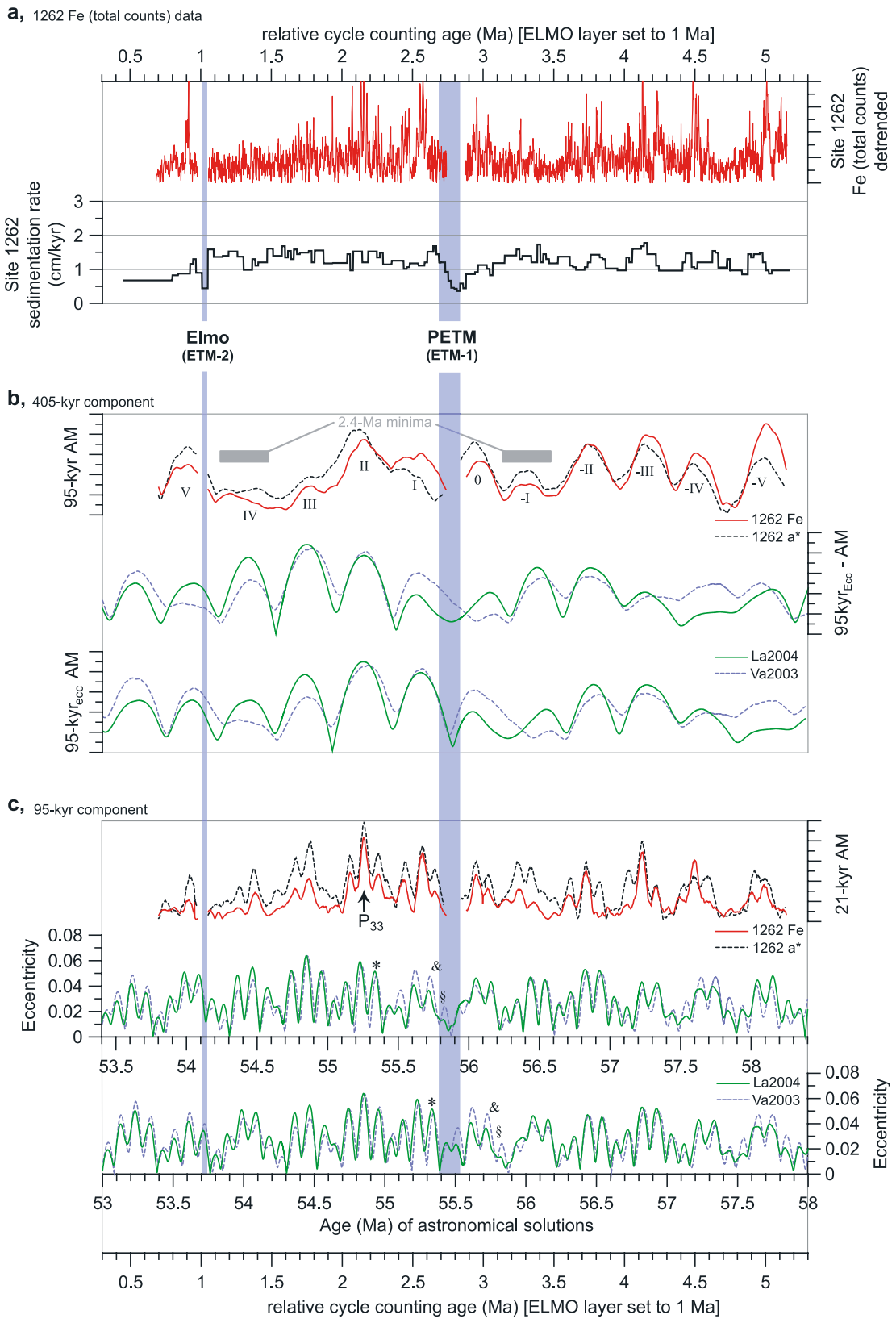

* age onset PETM Wing et al. (2000)
§ age onset PETM GTS2004 (Gradstein et al. 2004)
& recalibrated radiometic age estimate of the onset PETM

Figure 6

acterized by the lowest sedimentation rates (~0.5 cm/kyr) [*Lourens et al.*, 2005; *Zachos et al.*, 2005].

[31] We extracted the amplitude modulation of short and long eccentricity from Site 1262 Fe and a* data using central filter periods of 21 and 95 kyr with ±15% bandwidth, respectively (Figures 6b and 6c). We used a window width factor (wfac) of 4 times the designated filter period, and a Welch taper-type window. The PETM and Elmo horizon were removed from the data set to avoid signal amplitude artifacts. The extracted short and long eccentricity paced signals (Figures 6b and 6c) show prominent amplitude modulations, although slight differences can be identified between the Fe and a* data. Given the higher sampling rate and lower signal-to-noise ratio the Fe data clearly provide a higher-fidelity record of orbital variations. The most important feature is the presence of two minima in the very long eccentricity cycle at ~1.25 Ma (IV) and ~3.3 Ma (−I) according to the relative timescale (Figure 6b). These can be easily identified in all data sets as intervals of very low-amplitude modulation of the climatic precession cycles (see Figures 4a and 4b). The second important feature is the lack of a transition in the eccentricity and precession-amplitude-modulation period from ~2.4 to ~1.2 Myr between 53 and 58 Ma. The detection of the first transition from a ~2.4 to ~1.2 Myr period is though to provide some extreme constraint for the gravitational model of the Solar System and therefore future orbital solutions (for discussion see *Laskar et al.* [2004] and *Pälike et al.* [2004]). A final feature is related to the alignment of the onset of the PETM and the ETM2 relative to the short- and long-term eccentricity cycles. While the PETM aligns with a decreasing branch of a 405-kyr eccentricity cycle, the ETM2 falls at a increasing branch, not with a 405-kyr maximum [*Lourens et al.*, 2005] or a 405-kyr minimum [*Cramer et al.*, 2003] as previously speculated. Nevertheless, both events seem to be related to a short eccentricity maximum as proposed by *Lourens et al.* [2005].

[32] Subsequently a tentative comparison was made between the extracted amplitude modulations of a* and Fe records, and the current available astronomical solutions (Figure 6b). This may provide a first-order positioning of the Walvis Ridge records with respect to absolute ages. The two solutions, La2004 and Va2003, are almost identical for the 405-kyr component of orbital eccentricity in the period between 58.4 and 53 Ma (Figure 6b), while they differ for both the short-term (~100 kyr) and the very long-term (~2.4 Myr) components of eccentricity [*Laskar et al.*, 2004]. For example a minimum in the long-term (~2.4 Myr) component of eccentricity occurs around 55.7 Ma in La2004, but around 56.1 Ma in Va2003 (Figure 6). The similarity of both solutions in this period might be due to the fact that both are adjusted to the Jet Propulsion Laboratory ephemeris DE406. Because of uncertainties in the astronomical computations [*Laskar et al.*, 2004] and in radiometric dating for this time interval [*Machlus et al.*, 2004], only a floating timescale can be constructed using the stability of the 405-kyr eccentricity cycle as constraint.

[33] Starting point for tuning is the estimate of 55.3 Ma for the PETM in the Bighorn Basin [*Wing et al.*, 2000] based on the magnetostratigraphy [*Tauxe et al.*, 1994], biostratigraphy [*Wing*, 1984], and an $^{40}Ar/^{39}Ar$ age of 52.8 ± 0.16 Ma [*Wing et al.*, 1991] for the base of chron C24n.1n [*Tauxe et al.*, 1994]. To align our records with the stable 405-kyr cycle, however, we have to shift them ~200 kyr relative to that estimate in either direction. The best fit was obtained by aligning precession cycle 33 to the age datum of 54.850 Ma, which lies close to a maximum in the 405-kyr cycle (Figure 6c). This is reflected in the comparison of the demodulated 405-kyr and 95-kyr amplitude component of the precession cycles in the Fe and a* data with the two eccentricity solutions (Figure 6c). If we assume that the eccentricity solutions La2004 and Va2003 are correct, all other options must be rejected, because the ages of the PETM and reversal boundaries would deviate by more than 1.6 Ma from published estimates [*Cande and Kent*, 1992, 1995; *Lourens et al.*, 2005; *Ogg and Smith*, 2004]. Applying the eccentricity solutions La2004 and Va2003 and correlating our data to them we would derive an absolute age of ~55.53 Ma for the PETM and ~53.69 Ma for the ETM2 (Table 3). In this case, magnetochron C25n would have lasted from ~57.16 Ma to ~56.65 Ma, and C24r from ~56.65 Ma to ~53.53 Ma. The error given in Table 3

Figure 6. Comparison of relative cycle counting timescale with present astronomical solutions for orbital eccentricity. (a) Results of relative timescale: Site 1262 detrended Fe intensity data (red line) using a high-pass filter versus relative cycle counting age in Ma. We assume that the mean duration of one precession cycle is 21.0 kyr, and we set the Elmo horizon arbitrarily to 1.0 Ma. The resulting sedimentation rates in cm/kyr show minor variations throughout the record. In contrast, the regions containing the Elmo horizon and the PETM reveal lower than mean sedimentation rates because of strong dissolution of calcium carbonates (for discussion see *Lourens et al.* [2005] and *Zachos et al.* [2005]). (b) and (c) Comparison of current astronomical solutions plotted against absolute time and the extracted amplitude modulation of Site 1262 data plotted against relative time. We have shifted the Site 1262 data with respect to the best fit with the 405-kyr cycle; for further explanation, see text. Short eccentricity cycle amplitude modulation of Site 1262 Fe intensity (red) data, a* (dashed black) data, the La2004 [*Laskar et al.*, 2004] (green), and Va2003 [*Varadi et al.*, 2003] (dashed blue) orbital eccentricity solutions (Figure 6b). For comparison the La2004 and Va2003 amplitude modulation have been plotted from 53 to 58 Ma (bottom plot) and 53.4 to 58.4 Ma (middle plot). Climatic precession cycle amplitude modulation of Site 1262 data (Fe in red and a* in dashed black) compared to orbital eccentricity solutions La2004 (green) and Va2003 (dashed blue) from 53 to 58 Ma (bottom plot) and 53.4 to 58.4 Ma (middle plot) (Figure 6c). Additionally, the 2.4 Ma eccentricity minima in Site 1262 data are marked (see text for discussion). The amplitude modulations have been extracted with the program ENVELOPE [*Schulz et al.*, 1999]. Different proposed absolute ages for the onset of the PETM are also shown; for discussion see text.

Table 3. Estimates of Absolute Age of Magnetochrons and Global Events[a]

Chron (Event)	Estimated Age, Ma		Duration, Myr
	Option 1	Option 2	
C24r			3.118 ± 0.05[b]
C24r (y)	53.53 ± 0.04[c]	53.93 ± 0.04[c]	
C24r (o)	56.65 ± 0.01[c]	57.05 ± 0.01[c]	
C25n			0.511 ± 0.05[b]
C25n (y)	56.65 ± 0.01[c]	57.05 ± 0.01[c]	
C25n (o)	57.16 ± 0.04[c]	57.56 ± 0.04[c]	
Elmo (ETM-2)	53.69 ± 0.02[b]	54.09 ± 0.02[b]	
PETM (ETM-1)[d]	55.53 ± 0.02[b]	55.93 ± 0.02[b]	

[a]Abbreviations are y, younger; and o, older.
[b]Errors take into account only the uncertainty in cycle counting; error associated with the orbital solution not added.
[c]Errors take into account only the uncertainty of the position of magnetic reversal boundaries.
[d]Onset of carbon excursion.

refers to the uncertainty in cycle counting as discussed above and the position of the reversal boundary in the data sets. In contrast, according to the GTS2004 the age of the PETM is ~55.8 Ma, thus 300kyr older than our first estimate. In the following section we will discuss some of the uncertainties in estimating the absolute age for the PETM.

5.5. Age for the PETM

[34] An absolute age of the PETM has been in a constant state of flux for the last few decades [e.g., see *Aubry et al.*, 1996; *Wing et al.*, 2000]. The age uncertainties are based on inconsistencies between biochronology and magnetochronology [*Aubry et al.*, 1996; *Berggren and Aubry*, 1996; *Berggren et al.*, 1995; *Norris and Röhl*, 1999; *Raffi et al.*, 2005; *Wing et al.*, 2000] and the way the CK95 Geomagnetic Polarity Timescale (GPTS) was constructed [*Berggren and Aubry*, 1996]. In contrast to CK95 the new GPTS2004 [*Ogg and Smith*, 2004] utilize radiometric calibration points in the late Paleocene–early Eocene at 52.8 Ma (base of C24n.1n) and 55.07 Ma (C24r.50), and dismiss the calibration point used in CK95 of 55.0 Ma for the Paleocene-Eocene boundary, which was deemed inappropriate [*Aubry et al.*, 1996]. The calibration point C24r.50 is located approximately in the middle of C24r [*Ogg and Smith*, 2004] constrained by $^{40}Ar/^{39}Ar$ ages and magnetostratigraphy of DSDP Hole 550 [*Swisher and Knox*, 1991]. The $^{40}Ar/^{39}Ar$ date from the middle of polarity chron C24r, which is significantly above the Paleocene-Eocene boundary, is derived from ash −17 with an age of 55.07 ± 0.5 Ma derived by J. D. Obradovich (see postscript given by *Berggren et al.* [1995]). New $^{40}Ar/^{39}Ar$ ages for ash −17 (54.96 ± 0.16 Ma [*Bird et al.*, 2003]) support the estimate of ~55.0 Ma for the middle of chron C24r.

[35] According to our youngest estimate (option 1, see Table 3), the absolute age of the middle of chron C24r (C24r.50) is ~55.09 Ma, which is very close to the radiometric dated ages. However, in case the radiometric dates of the −17 and +19 tephra are recalibrated to the Fish Canyon Tuff (FCT) $^{40}Ar/^{39}Ar$ standard age of 28.02 Ma [*Villeneuve*, 2004], this would result in an age of 55.3–55.4 Ma for the PETM (2/3 down in C24r). This is close to the estimate of 55.315 Ma (age model 2) by *Wing et al.* [2000] which does not rely on any marine calibration points in the late Paleocene and early Eocene. More recently, *Kuiper et al.* [2004, 2005] estimated an older age of 28.21 ± 0.04 Ma for the FCT based on the intercomparison with astronomical-derived ages for Miocene tephra layers. Accordingly, the age of the PETM would be ~55.75 Ma and that of C24r.50 ~55.4 Ma. Tuning the Walvis Ridge record one 405-kyr eccentricity cycle older (which theoretically we could do because of the uncertainties of the orbital solutions) would imply an age of the PETM of ~55.93 Ma (Figure 6c) and C24r.50 of ~55.49 Ma. If this is correct, this implies that the recalibrated Ar/Ar ages would still be too young by ~200kyr for the PETM. One explanation for the orbital-radiometric discrepancy that we are struggling with might be the observation that U-Pb and $^{207}Pb/^{206}Pb$ dates are older than $^{40}Ar/^{39}Ar$ by <1% (for discussion see *Schoene et al.* [2006]). Unfortunately, because of the relatively large errors in radiometric dating it is still impossible to verify if U-Pb dates are systematically <1% older than $^{40}Ar/^{39}Ar$ [*Schoene and Bowring*, 2006; *Schoene et al.*, 2006].

[36] If we assume the PETM to be at ~55.93 Ma (option 2) and compare the demodulated precession signal of the Walvis Ridge record with the two eccentricity solutions (Figure 6b) from 53.4 to 58.4 Ma than the prominent 2.4 Ma minima in the Walvis Records would coincide with intervals of high-amplitude variability in the La2004 and Va2003 solutions. The comparison of the geological data with the eccentricity solutions then would clearly suggest that the La2004 and Va2003 solution, especially the 2.4-Myr modulation, are not correct in the interval from ~53 to ~59 Ma. This would simply mean that orbital tuning to precession and eccentricity solutions in this interval is not possible. On the other hand, if we assume that the orbital solutions are correct and the best fit with the geological data gives the correct age for the PETM (~55.53 Ma), then the recalibrated Ar/Ar ages are too old. Owing to the uncertainty in the determination of the successive minima in the very long eccentricity cycle a direct anchoring of the studied interval to current orbital solutions is not possible. Therefore accurate absolute ages for the PETM and the C24r boundaries cannot be provided in the moment. To establish a robust absolute chronology and further insights in radiometric uncertainties new orbital solutions which are stable beyond 50 Ma are required. In addition, a cyclostratigraphic framework based on the stable long eccentricity cycle for the entire Paleogene has to be constructed, and the exact age of the FCT standard monitor has to be established. Until then, at least two different options for the absolute age of the onset of the PETM should be considered (~55.53 Ma, ~55.93 Ma).

6. Conclusion

[37] The deep-sea cores recovered in multiple holes during ODP Leg 208 at Walvis Ridge have yielded in the first complete high-resolution stratigraphic record for the early Paleogene and thus provides a continuous cyclostratigraphy for magnetochron C24r down to the precession

cycle scale. Detailed spectral analyses in the depth domain of both physical properties and geochemical sediment parameters from Sites 1262, 1263, 1265 and 1267 reveal that the late Paleocene and early Eocene sediments from the Walvis Ridge were clearly deposited in a cyclical fashion paced by orbital-driven climate processes. The ~ 4.3-Myr-long record is dominated by short- and long-term eccentricity modulated precession cycles, which provide the necessary framework to establish for the first time a tuned astronomical timescale for all sites. According to our cycle counting of Leg 208 sites and ODP Site 1051, the studied interval covers 200 precession cycles. Chrons C24r and C25n are the time equivalent of 148 and 23 precession cycles, respectively. Assuming a mean duration of 21 kyr per precession cycle the magnetochrons C24r and C25n are 3.108 and 0.483 Myr long. Chron C24r therefore is longer than previously estimated. The newly defined duration of chron 25n is in very good agreement with a previously published estimate [*Röhl et al.*, 2003].

[38] Moreover, the cyclestratigraphy provides the exact positions of critical intervals like the PETM and ETM2 within chron C24r for identifying these events in other marine- and land-based sections. The relative position of the PETM (at C24r.64) is in agreement with estimates from land-based sections [*Wing et al.*, 2000]. The records also show that the interval between the PETM and the ETM2 (at C24r.05) covers ~1.827 Myr rather than the ~2 Myr as initially estimated from the Leg 208 sites [*Lourens et al.*, 2005] and that both events cannot fall within the same phase of the long eccentricity cycle. The refined chronology results from the higher-fidelity signal provided by Fe intensities measurements obtained from XRF core logging, and by the inclusion of data from the shallower Sites 1263 and 1265. These sites have a much higher sedimentation rate resulting in a distinctly clearer signal in intervals where the Milankovitch cyclicity is much less pronounced. This allowed counting of individual precession and eccentricity cycles which gave a consistent duration of time between the PETM and ETM2. The amplitude modulation of the precession signal in Leg 208 sites also clearly shows that both the PETM and the ETM2 do not coincide with a maximum or a minimum in the long eccentricity cycle. However, both events are associated with a maximum in the short eccentricity cycle. This supports a possible astronomical triggering mechanism (threshold) of the early Eocene thermal events, rather then a stochastic process (i.e., bolide impact [*Kent et al.*, 2003]).

[39] In order to obtain an absolute age estimate for the PETM, the ETM2 and the magnetochron boundaries, the geological data have been compared to the current available astronomical solutions for orbital eccentricity [*Laskar et al.*, 2004; *Varadi et al.*, 2003]. Integration with recalibrated radiometric age estimates of the PETM gave inconsistent results. We conclude that robust absolute age estimates that are consistent with recalibrated Ar/Ar ages and recent models of Earth's orbital eccentricity cannot be provided by now. Given the uncertainty in radiometric dating a cyclostratigraphic framework based on the stable 405-kyr eccentricity cycle for the entire Paleogene is needed to pin down the absolute age of the PETM and geomagnetic polarity boundaries. This then will allow us to gain new insight in the Fish Canyon Tuff (FCT) $^{40}Ar/^{39}Ar$ standard age controversy and evaluate the accuracy of solutions for the Earth's orbital eccentricity.

[40] **Acknowledgments.** Funding for this research was provided by the Deutsche Forschungsgemeinschaft (DFG) to U. Röhl and T. Westerhold; by the Joint Oceanographic Institutions/United States Science Support Program to J. Bowles; by the National Science Foundation (NSF) to J. C. Zachos; by the Netherlands Organization for Scientific Research to L. J. Lourens; and by Italian Murst-PRIN to I. Raffi. We are indebted to H. Pfletschinger (Bremen) for assisting in XRF scanning Leg 208 cores and thank A. Wülbers and W. Hale (ODP/IODP Bremen Core repository) for core handling. We also thank three anonymous reviewers for comments that improved the manuscript. This research used samples and data provided by the Ocean Drilling Program (ODP). ODP is sponsored by the U.S. National Science Foundation (NSF) and participating countries under the management of Joint Oceanographic Institution (JOI), Inc. The complete data set presented in this paper is available online in the WDC-MARE PANGAEA database under www.pangaea.de.

References

Aubry, M.-P. (1999), Late Paleocene-early Eocene sedimentary history in western Cuba: Implications for the LPTM and regional tectonic history, *Micropaleontology*, *45*, 5–18.

Aubry, M.-P., W. A. Berggren, L. D. Stott, and A. Sinha (1996), The upper Paleocene-lower Eocene stratigraphic record and the Paleocene-Eocene boundary carbon isotope excursion: Implications for geochronology, in *Correlation of the Early Paleogene in Northwest Europe*, edited by R. W. O. B. Knox, R. M. Corfield, and R. E. Dunay, *Spec. Publ. Geol. Soc.*, *101*, 353–380.

Backman, J., and I. Raffi (1997), Calibration of Miocene nannofossil events to orbitally tuned cyclostratigraphies from Ceara Rise, *Proc. Ocean Drill. Program, Sci. Results*, *154*, 83–99.

Backman, J., and N. J. Shackleton (1983), Quantitative biochronology of Pliocene and early Pleistocene calcareous nannofossils from the Atlantic, Indian and Pacific Ocean, *Mar. Micropaleontol.*, *8*, 141–170.

Bains, S., R. D. Norris, R. M. Corfield, G. J. Bowen, P. D. Gingerich, and P. L. Koch (2003), Marine-terrestrial linkages at the Paleocene-Eocene boundary, in *Causes and Consequences of Globally Warm Climates in the Early Paleogene*, edited by S. L. Wing et al., *Spec. Pap. Geol. Soc. Am.*, *369*, 1–9.

Berger, A., M. F. Loutre, and J. Laskar (1992), Stability of the astronomical frequencies over the Earth's history for paleoclimate studies, *Science*, *255*, 560–566.

Berggren, W. A., and M.-P. Aubry (1996), A late Paleocene-early Eocene NW European and North Sea magnetobiochronology correlation network, in *Correlation of the Early Paleogene in Northwest Europe*, edited by R. W. O. B. Knox, R. M. Corfield, and R. E. Dunay, *Spec. Publ. Geol. Soc.*, *101*, 309–352.

Berggren, W. A., D. V. Kent, C. C. Swisher III, and M. P. Aubury (1995), A revised Cenozoic geochronology and chronostratigraphy, in *Geochronology, Time Scales and Global Stratigraphic Correlation*, edited by W. A. Berggren et al., *Spec. Publ. Soc. SEPM Sediment. Geol.*, *54*, 129–212.

Bird, D. K., L. E. Heister, C. K. Brooks, and C. Tegner (2003), Linking tephras and Paleocene-Eocene paleoclimate of Denmark to flood and Plinian volcanism of East Greenland (abstract), *Geophys. Res. Abstr.*, *5*, 14310.

Bukry, D. (1973), Low-latitude coccolith biostratigraphic zonation, *Initial Rep. Deep Sea Drill. Proj.*, *15*, 685–703.

Bukry, D. (1978), Coccolith and silicoflagellate stratigraphy, northwestern Pacific Ocean, Deep Sea Drilling Project Leg 32, *Initial Rep. Deep Sea Drill. Proj.*, *32*, 677–701.

Cande, S. C., and D. V. Kent (1992), A new geomagnetic polarity time scale for the Late Cretaceous and Cenozoic, *J. Geophys. Res.*, *97*, 13,917–13,951.

Cande, S. C., and D. V. Kent (1995), Revised calibration of the geomagnetic polarity time-

scale for the Late Cretaceous and Cenozoic, *J. Geophys. Res.*, *100*, 6093–6095.

Cramer, B. S. (2001), Latest Paleocene-earliest Eocene cyclostratigraphy: Using core photographs for reconnaissance geophysical logging, *Earth Planet. Sci. Lett.*, *186*, 231–244.

Cramer, B. S., J. D. Wright, D. V. Kent, and M.-P. Aubry (2003), Orbital climate forcing of $\delta^{13}C$ excursions in the late Paleocene–Eocene (chrons C24n–C25n), *Paleoceanography*, *18*(4), 1097, doi:10.1029/2003PA000909.

Dehant, V., M. F. Loutre, and A. Berger (1987), Les variations à court et à long terme de la rotation de la Terre et de la précession astronomique, *Rep.87/12*, Inst. d'Astron. et de Géophys. Lémâitre, G., Univ. Cath. de Louvain, Louvain-la-Neuve, France.

Dinarès-Turell, J., J. I. Baceta, V. Pujalte, X. Orue-Etxebarria, and G. Bernaola (2002), Magnetostratigraphic and cyclostratigraphic calibration of a prospective Palaeocene/Eocene stratotype at Zumaia (Basque Basin, northern Spain), *Terra Nova*, *14*, 371–378.

Evans, H. F., T. Westerhold, and J. E. T. Channell (2004), ODP Site 1092: Revised composite depth section has implications for Upper Miocene 'cryptochron', *Geophys. J. Int.*, *156*, 195–199.

Farley, K. A., and S. F. Eltgroth (2003), An alternative age model for the Paleocene-Eocene thermal maximum using extraterrestrial ^{3}He, *Earth Planet. Sci. Lett.*, *208*, 135–148.

Ferraz-Mello, S. (1981), Estimation of periods from unequally spaced observations, *Astron. J.*, *86*, 619–624.

Gradstein, F., J. Ogg, and A. Smith (2004), *A Geological Timescale 2004*, Cambridge Univ. Press, New York.

Hallam, A., J. M. Hancock, J. L. LaBreque, W. Lowrie, and J. E. T. Channell (1985), Jurassic to Paleogene: part I. Jurassic and Cretaceous geochronology and Jurassic to Palaeogene magnetostratigraphy, in *The Chronology of the Geological Record*, edited by N. J. Snelling, pp. 118–140, Geological Society, London.

Herbert, T. D., I. Premoli-Silva, E. Erba, and A. G. Fischer (1995), Orbital chronology of Cretaceous-Paleocene marine sediments, in *Geochronology, Time Scales and Global Stratigraphic Correlation*, edited by W. A. Berggren et al., *Spec. Publ. SEPM Sediment. Geol.*, *54*, 81–93.

Hilgen, F. (1991), Extension of the astronomically calibrated (polarity) time scale to the Miocene/Pliocene boundary, *Earth Planet. Sci. Lett.*, *107*, 349–368.

Hilgen, F. J., et al. (1999), Present status of the astronomical (polarity) time-scale for the Mediterranean late Neogene, *Philos. Trans. R. Soc. London, Ser. A*, *357*, 1931–1947.

Hinnov, L. A. (2000), New perspectives on orbitally forced stratigraphy, *Annu. Rev. Earth Planet. Sci.*, *28*, 419–475.

Hinnov, L. A. (2004), Earth's orbital parameters and cycle stratigraphy, in *A Geological Timescale 2004*, edited by F. Gradstein, J. Ogg, and A. Smith, pp. 55–62, Cambridge Univ. Press, New York.

Jansen, J. H. F., S. J. Van der Gaast, B. Koster, and A. J. Vaars (1998), CORTEX, a shipboard XRF-scanner for element analyses in split sediment cores, *Mar. Geol.*, *151*, 143–153.

Katz, M. E., D. K. Pak, G. R. Dickens, and K. G. Miller (1999), The source and fate of massive carbon input during the latest Paleocene thermal maximum, *Science*, *286*, 1531–1533.

Kennett, J. P., and L. D. Stott (1991), Abrupt deep sea warming, paleoceanographic changes and benthic extinctions at the end of the Paleocene, *Nature*, *353*, 225–229.

Kent, D. V., B. S. Cramer, L. Lanci, D. Wang, J. D. Wright, and R. Van der Voo (2003), A case for a comet impact trigger for the Paleocene/Eocene thermal maximum and carbon isotope excursion, *Earth Planet. Sci. Lett.*, *211*, 13–26.

Kirschvink, J. L. (1980), The least-squares line and plane and the analysis of paleomagnetic data, *Geophys. J. R. Astron. Soc.*, *62*, 699–718.

Koch, P. L., J. C. Zachos, and P. Gingerich (1992), Correlation between isotope records in marine and continental carbon reservoirs near the Paleocene/Eocene boundary, *Nature*, *358*, 319–322.

Kuiper, K. F., F. J. Hilgen, J. Steenbrink, and J. R. Wijbrans (2004), $^{40}Ar/^{39}Ar$ ages of tephras intercalated in astronomically tuned Neogene sedimentary sequences in the Mediterranean, *Earth Planet. Sci. Lett.*, *222*, 583–597.

Kuiper, K. F., J. R. Wijbrans, and F. J. Hilgen (2005), Radioisotopic dating of the Tortonian global stratotype section and point: Implications for intercalibration of $^{40}Ar/^{39}Ar$ and astronomical dating methods, *Terra Nova*, *17*, 385–398.

Laskar, J. (1999), The limits of Earth orbital calculations for geological time-scale use, *Philos. Trans. R. Soc. London, Ser. A*, *357*, 1735–1759.

Laskar, J., P. Robutel, F. Joutel, M. Gastineau, A. Correia, and B. Levrard (2004), A long-term numerical solution for the insolation quantities of the Earth, *Astron. Astrophys.*, *428*, 261–285.

Lourens, L. J., A. Sluijs, D. Kroon, J. C. Zachos, E. Thomas, U. Röhl, J. Bowles, and I. Raffi (2005), Astronomical pacing of late Palaeocene to early Eocene global warming events, *Nature*, *435*, 1083–1087.

Luterbacher, H. P., J. Hardenbol, and B. Schmitz (2000), Decision of the voting members of the International Subcommission on Paleogene Stratigraphy on the criterion of recognition of the Paleocene/Eocene boundary, *Newsl. Int. Subcommi.Paleogene Stratigr.*, *9*, 13 pp.

Machlus, M., S. R. Hemming, P. E. Olsen, and N. Christie-Blick (2004), Eocene calibration of geomagnetic polarity time scale reevaluated: Evidence from the Green River Formation of Wyoming, *Geology*, *32*, 137–140.

Martini, E. (1971), Standard Tertiary and Quaternary calcareous nannoplankton zonation, in *Proceedings of 2nd International Conference Planktonic Microfossils Roma*, edited by A. Farinacci, pp. 739–785, Tecnosci., Rome.

Néron de Surgy, O., and J. Laskar (1997), On the long term evolution of the spin of the Earth, *Astron. Astrophys.*, *318*, 975–989.

Norris, R. D., and U. Röhl (1999), Carbon cycling and chronology of climate warming during the Palaeocene/Eocene transition, *Nature*, *401*, 775–778.

Norris, R. D., et al.(1998) *Black Nose Paleoceanographic Transect, Western North Atlantic*, 1–749 pp., Ocean Drill. Program, College Station, Tex.

Ogg, J. G., and L. Bardot (2001), Aptian through Eocene magnetostratigraphic correlation of the Blake Nose Transect (Leg 171B), Florida continental margin [online], *Proc. Ocean Drill. Program Sci. Results*, *171B*, 1–58. (Available at http://www-odp.tamu.edu/publications/171B_SR/chap_09/chap_09.htm)

Ogg, J. G., and A. G. Smith (2004), The geomagnetic polarity time scale, in *A Geological Timescale 2004*, edited by F. Gradstein, J. Ogg, and A. Smith, pp. 63–86, Cambridge Univ. Press, New York.

Paillard, D., L. Labeyrie, and P. Yiou (1996), Macintosh program performs time-series analysis, *Eos Trans. AGU*, *77*, 379. (Available at http://www.agu.org/eos_elec/96097e.html)

Pälike, H., J. Laskar, and N. J. Shackleton (2004), Geologic constraints on the chaotic diffusion of the solar system, *Geology*, *32*, 929–932.

Raffi, I., J. Backman, and H. Pälike (2005), Changes in calcareous nannofossil assemblages across the Paleocene/Eocene transition from the paleo-equatorial Pacific Ocean, *Palaeogeogr. Palaeoclimatol. Palaeoecol.*, *226*, 93–126.

Rio, D., I. Raffi, and G. Villa (1990), Pliocene-Pleistocene calcareous nannofossil distribution patterns in the Mediterranean, *Proc. Ocean Drill. Program Sci. Results*, *107*, 513–533.

Röhl, U., and L. J. Abrams (2000), High-resolution, downhole and non-destructive core measurements from Sites 999 and 1001 in the Caribbean Sea: Application to the late Paleocene thermal maximum, *Proc. Ocean Drill. Program Sci. Results*, *165*, 191–203.

Röhl, U., T. J. Bralower, R. D. Norris, and G. Wefer (2000), New chronology for the late Paleocene thermal maximum and its environmental implications., *Geology*, *28*, 927–930.

Röhl, U., R. D. Norris, and J. G. Ogg (2003), Cyclostratigraphy of upper Paleocene and lower Eocene sediments at Blake Nose Site 1051 (western North Atlantic), in *Causes and Consequences of Globally Warm Climates in the Early Paleogene*, edited by S. L. Wing et al., *Spec. Pap. Geol. Soc. Am.*, 369, 576–589.

Röhl, U., T. Westerhold, T. J. Bralower, M.-R. Petrizzo, and J. C. Zachos (2004), An early late Paleocene global dissolution event and new constraints for an astronomically-tuned early Paleogene time scale, paper presented at 8th International Conference on Paleoceanography, Environ. et Paleoenviron. Ocean., Biarritz, France.

Röhl, U., T. Westerhold, S. Monechi, E. Thomas, J. C. Zachos, and B. Donner (2005), The third and final early Eocene thermal maximum: Characteristics, timing and mechanisms of the "X" event, paper presented at Annual Meeting, Geol. Soc. of Am., Salt Lake City, Utah.

Schmitz, B., V. Pujalte, and K. Nunez-Betelu (2001), Climate and sea-level perturbation during the initial Eocene thermal maximum: Evidence from siliciclastic units in the Basque Basin (Ermua, Zumaia and Trabakua Pass), *Palaeogeogr. Palaeoclimatol. Palaeoecol.*, *165*, 299–320.

Schoene, B., and S. A. Bowring (2006), U-Pb systematics of the McClure Mountain syenite: Thermochronological constraints on the age of the $^{40}Ar/^{39}Ar$ standard MMhb, *Contrib. Mineral.Petrol.*, *151*, 615–630.

Schoene, B., J. L. Crowley, D. J. Condon, M. D. Schmitz, and S. A. Bowring (2006), Reassessing the uranium decay constants for geochronology using ID-TIMS U-Pb data, *Geochim. Cosmochim. Acta*, *70*, 426–445.

Schulz, M., W. H. Berger, M. Sarnthein, and P. M. Grootes (1999), Amplitude variations of 1470-year climate oscillations during the last 100,000 years linked to fluctuations of continental ice mass, *Geophys. Res. Lett.*, *26*, 3385–3388.

Shackleton, N. J., and S. Crowhurst (1997), Sediment fluxes based on an orbitally tuned time scale 5 to 14 Ma, Site 926, *Proc. Ocean Drill. Program Sci. Results*, *154*, 69–82.

Shackleton, N. J., T. King Hagelberg, and S. J. Crowhurst (1995), Evaluating the success of astronomical tuning: Pitfalls of using coherence as a criterion for assessing pre-Pleistocene timescales, *Paleoceanography*, *10*, 693–697.

Shackleton, N. J., S. J. Crowhurst, G. P. Weedon, and J. Laskar (1999), Astronomical calibration of Oligocene-Miocene time, *Philos. Trans. R. Soc. London A*, *357*, 1907–1929.

Shackleton, N. J., M. A. Hall, I. Raffi, L. Tauxe, and J. Zachos (2000), Astronomical calibration age for the Oligocene-Miocene boundary, *Geology*, *28*, 447–450.

Shipboard Scientific Party (2004a), Explanatory notes, *Proc. Ocean Drill. Program Initial Rep.* [CD-ROM], *208*, 1–63.

Shipboard Scientific Party (2004b), Leg 208 summary, *Proc. Ocean Drill. Program Initial Rep.* [CD-ROM], *208*, 1–112.

Shipboard Scientific Party (2004c), Site 1262, *Proc. Ocean Drill. Program Initial Rep.* [CD-ROM], *208*, 1–92.

Shipboard Scientific Party (2004d), Site 1263, *Proc. Ocean Drill. Program Initial Rep.* [CD-ROM], *208*, 1–87.

Shipboard Scientific Party (2004e), Site 1265, *Proc. Ocean Drill. Program Initial Rep.* [CD-ROM], *208*, 1–107.

Shipboard Scientific Party (2004f), Site 1267, *Proc. Ocean Drill. Program Initial Rep.* [CD-ROM], *208*, 1–77.

Swisher, C. C. III, and R. W. O. B. Knox (1991), The age of the Paleocene/Eocene boundary: $^{40}Ar/^{39}Ar$ dating of the lower part of NP10, North Sea Basin and Denmark, paper presented at International Geological Correlation Project 308 Meeting, Brussels, Belgium.

Tauxe, L., J. Gee, Y. Gallet, T. Pick, and T. Bown (1994), Magnetostratigraphy of the Willwood Formation, Bighorn Basin, Wyoming: New constraints on the location of Paleocene/Eocene boundary, *Earth Planet. Sci. Lett.*, *125*, 159–172.

Tauxe, L., T. Pick, and Y. S. Kok (1995), Relative paleointensity in sediments: A pseudo-Thellier approach, *Geophys. Res. Lett.*, *22*, 2885–2888.

Tripati, A. K., M. L. Delaney, J. C. Zachos, L. D. Anderson, D. C. Kelly, and H. Elderfield (2003), Tropical sea-surface temperature reconstruction for the early Paleogene using Mg/Ca ratios of planktonic foraminifera, *Paleoceanography*, *18*(4), 1101, doi:10.1029/2003PA000937.

Varadi, F., B. Runnegar, and M. Ghil (2003), Successive refinements in long-term integrations of planetary orbits, *Astrophys. J.*, *592*, 620–630.

Villeneuve, M. (2004), Radiogenic isotope geochronology, in *A Geological Timescale 2004*, edited by F. Gradstein, J. Ogg, and A. Smith, pp. 87–95, Cambridge Univ. Press, New York.

Weedon, G. P. (1993), The recognition and stratigraphic implications of orbital-forcing of climate and sedimentary cycles, *Sedimentology Review*, edited by V. P. Wright et al., pp. 31–50, Blackwell Sci., Malden, Mass.

Weedon, G. P. (2003), *Time-Series Analysis and Cyclostratigraphy*, 259 pp., Cambridge Univ. Press, New York.

Wing, S. L. (1984), A new basis for recognizing the Paleocene/Eocene boundary in western interior North America, *Science*, *226*, 439–441.

Wing, S. L., T. M. Brown, and J. D. Obradovich (1991), Early Eocene biotic and climatic change in interior western North America, *Geology*, *19*, 1189–1192.

Wing, S. L., H. Bao, and P. L. Koch (2000), An early Eocene cool period? Evidence for continental cooling during the warmest part of the Cenozoic, in *Warm Climates in Earth History*, edited by B. T. Huber, K. G. MacLeod, and S. L. Wing, pp. 197–237, Cambridge Univ. Press, New York.

Zachos, J. C., et al. (2004), *Proceedings of the Ocean Drilling Program Initial Report* [CD-ROM], vol. 208, Ocean Drill. Program, College Station, Tex.

Zachos, J. C., et al. (2005), Rapid acidification of the ocean during the Paleocene-Eocene thermal maximum, *Science*, *308*, 1611–1615.

J. Bowles, Scripps Institution of Oceanography, University of California, San Diego, 9500 Gilman Drive, MC0220, La Jolla, CA 92093, USA.

J. Laskar, Astronomie et Systèmes Dynamiques, IMCCE-CNRS UMR8028, 77 Av. Denfert-Rochereau, Paris F-75014, France.

L. J. Lourens, Faculty of Geosciences, Department of Earth Sciences, Utrecht University, Budapestlaan 4, Utrecht 3584 CD, Netherlands.

I. Raffi, Facoltà di Scienze, Dipartimento di Geotecnologie per l'Ambiente e il Territorio, Università "G. d'Annunzio" di Chieti-Pescara, Campus Universitario, Via dei Vestini 31, Chieti Scalo I-66013, Italy.

U. Röhl and T. Westerhold, Centre for Marine Environmental Sciences, Bremen University, Leobener Strasse, Bremen D-28359, Germany. (tho@uni-bremen.de)

J. C. Zachos, Earth and Planetary Sciences Department, University of California, Santa Cruz, Santa Cruz, CA 95064, USA.